Acta Mech 223, 2437–2458 (2012)
DOI 10.1007/s00707-012-0696-y

Yu-Fu Ko · J. W. Ju

New higher-order bounds on effective transverse elastic moduli of three-phase fiber-reinforced composites with randomly located and interacting aligned circular fibers

Received: 30 October 2011 / Revised: 2 March 2012 / Published online: 10 August 2012

Abstract A higher-order structure for three-phase composites containing randomly located yet unidirectionally aligned circular fibers is proposed to predict effective transverse elastic moduli based on the probabilistic spatial distribution of circular fibers, the pairwise fiber interactions, and the ensemble-area homogenization method. Specifically, the two inhomogeneity phases feature distinct elastic properties and sizes. In the special event, two-phase composites with same elastic properties and sizes of fibers are studied. Two non-equivalent formulations are considered in detail to derive effective transverse elastic moduli of two-phase composites leading to new higher-order bounds. Furthermore, the effective transverse elastic moduli for an incompressible matrix containing randomly located and identical circular rigid fibers and voids are derived. It is demonstrated that significant improvements in the singular problems and accuracy are achieved by the proposed methodology. Numerical examples and comparisons among our theoretical predictions, available experimental data, and other analytical predictions are rendered to illustrate the potential of the present method.

1 Introduction

Composite materials consist of two or more phases combined together on a macroscopic scale to form specific new materials with certain desirable material properties and enhanced engineering performance. The "inclusions" in composites can be of various forms such as fibers, whiskers, and particulates. The other primary phase in composites is named the "matrix." The matrix materials usually serve as the binder materials not only to support and protect the inclusions but also to transfer stresses between perfectly bonded and partially debonded/broken inclusions under three-dimensional complex loading. Composite materials can significantly improve such properties of a material as strength, stiffness, corrosion resistance, wear resistance, attractiveness, weight,

Y.-F. Ko (✉)
Department of Civil Engineering and Construction Engineering Management,
California State University, Long Beach, CA 90840-5101, USA
E-mail: Yu-Fu.Ko@csulb.edu
URL: http://www.csulb.edu/colleges/coe/cecem/views/personnel/fulltime/ko.shtml
Tel.: +1-562-9857884

J. W. Ju
College of Civil Engineering and Architecture,
Guangxi University, Nanning, China

J. W. Ju
Department of Civil and Environmental Engineering,
University of California, Los Angeles, CA 90095-1593, USA
E-mail: juj@ucla.edu
URL: http://www.cee.ucla.edu/faculty/ju/profile

fatigue life, temperature-dependent behavior, thermal insulation, thermal conductivity, acoustical insulation, etc.

Many theoretical methods have been developed in the literature to predict the effective elastic moduli of random heterogeneous multiphase fiber/particle reinforced composites. It can be divided into four major schools; that is, the variational method, the effective medium method, the *direct* micromechanical approach, and the finite element method. The variational method employs variational principles to obtain mathematical lower and upper bounds for effective elastic properties of composites within the linear elasticity theory. We refer to Hashin and Shtrikman [1,2], Hill [3,4], Hashin and Rosen [5], Hashin [6], Walpole [7–9], and Hashin [10]. Their method renders generally better bounds than the Voigt and Reuss bounds. The "improved" higher-order mathematical bounds (which depend on the statistical microstructural information of random heterogeneous composites) were also investigated by Silnutnzer [11], Milton [12], Milton and Phan-Thien [13], Torquato and Lado [14], etc. For example, Silnutzer [11] derived improved bounds on effective in-plane shear and bulk moduli. The Silnutzer bounds are referred to as the third-order (three-point) bounds. The effective medium method includes the self-consistent model, the differential scheme, the generalized self-consistent model, and the Mori-Tanaka model. We refer to Hill [15,16], Christensen and Lo [17], Mori and Tanaka [18], Benveniste [19], and Weng [20]. However, the effective medium methods as a group depend only on geometries of particles (inclusions) and volume fractions; they do not consider the spatial locations or probabilistic distributions of particles (inclusions). The effective medium methods are inherently independent of the spatial or statistical particles distribution, thus best suited for low particle concentrations or some limited special configurations. Special attention is given to the *direct* micromechanical approach. This approach, a closed-form solution, aims at direct micromechanical determination of effective properties of composites with randomly located and interacting inclusions by employing some approximations or with certain special geometric configurations for inclusions dispersed in matrix materials. Eshelby [21] considered an ellipsoidal inclusion embedded in infinite matrix and proposed the celebrated "Eshelby's equivalence principle". Mura [22] mainly considered rigorous "local" micromechanics, and there was no homogenization process involved. Honein [23] proposed a general framework to solve the problem of two circular inclusions in in-plane elastostatics, subjected to arbitrary loading by utilizing Kolosov-Muskhelishvili complex potentials. Furthermore, Nemat-Nasser and Hori [24] devoted and contributed to this approach. Nevertheless, only "local" field solutions can be obtained based upon the above approach. Based upon the work done by Eshelby [21], a micromechanical higher-order (in ϕ) ensemble-volume average formulation was proposed by Ju and Chen [25,26] to obtain the effective moduli of elastic multi-phase composites containing randomly dispersed ellipsoidal and spherical inhomogeneities, respectively. Both "local" and "overall" field solutions are obtained. The pairwise inclusion interactions were considered in their formulation. Therefore, the ensemble-volume averaged micromechanical field equations are formulated by the homogenization process from their approach. Along this line, Ju and Zhang [27], Ju and Yanase [28,29], and Lin and Ju [30] used a micromechanics approach to obtain effective elastic moduli of composites with randomly located aligned circular fibers or randomly dispersed spherical particles featuring *same/ distinct* elastic properties and *same sizes*. Due to the advent of high-speed computing machinery, the numerical solutions based on finite element methods are provided by the "unit cell model" where some periodic arrays of fibers are generally assumed. We refer to Adams and Crane [31], Nimmer et al. [32], Doghri and Friebel [33]. Emanating from the general framework of Ju and Chen [25,26], Ju and co-workers further investigated the micromechanics and effective elastoplastic behaviors of two-phase metal matrix composites [34–39], the exact formulation for the exterior-point Eshelby's tensor of an ellipsoidal inclusion [40], and micromechanical damage models for effective elastoplastic behaviors of ductile matrix composites accommodating evolutionary particle debonding/cracking and interfacial fiber debonding with/without thermal residual stress effects [41–56].

The primary objective of the present paper is to extend the framework of Ju and Zhang [27] and construct a *higher-order* framework to predict the effective transverse elastic moduli of two-phase fiber-reinforced composites based on the probabilistic spatial distribution of cylindrical fibers, pairwise fiber interactions, and the ensemble-area averaging procedure. All fibers are considered non-intersecting, randomly located, and embedded firmly in the matrix with perfect interfaces.

The remainder of the paper is organized as follows. In Sect. 2, we present approximate analytical solutions for the direct interactions between two different, randomly located elastic cylindrical fibers embedded in the matrix material. The two inclusion phases feature *distinct* elastic properties and sizes for the *three-phase* composites. Subsequently, the ensemble-area averaged eigenstrains are obtained through the probabilistic pairwise fiber interaction mechanism in Sect. 3. In addition, two non-equivalent formulations associated with *uniform* radial distribution function (URDF) and *general* radial distribution function (GRDF) are considered in detail

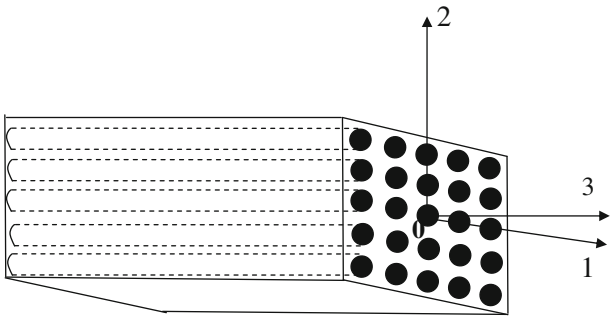

Fig. 1 A schematic plot of a composite reinforced by unidirectionally aligned yet randomly located cylindrical fibers

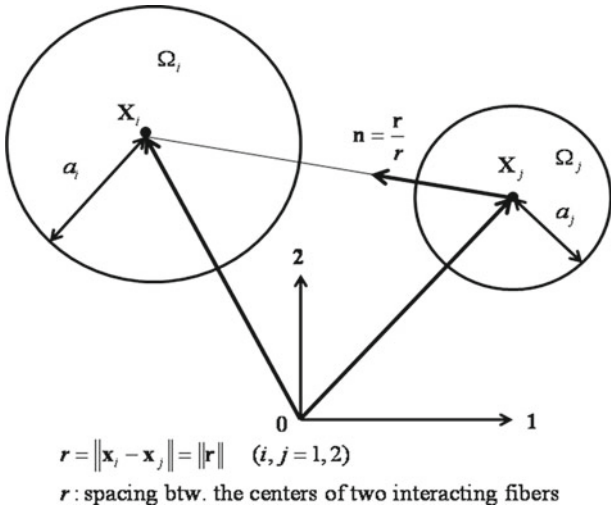

Fig. 2 The schematic diagram for the two-fiber interaction problem

to derive the ensemble-area averaged eigenstrains. In the special event, the effective elastic moduli of two-phase composites containing randomly located cylindrical fibers featuring *same* elastic properties and sizes are analytically derived in Sect. 4. Comparisons between our micromechanical predictions and other analytical predictions as well as experimental data are rendered in Sect. 5. As special case, a two-phase composite containing randomly located cylindrical rigid fibers and microvoids embedded in an elastic or in an incompressible matrix is also considered. We finally draw conclusions in Sect. 6.

2 Approximate local solutions of two interacting fibers

Let us consider a three-phase composite consisting of an isotropic elastic matrix (phase 0) with the plane-strain bulk modulus k_0 and the plane-strain shear modulus μ_0, randomly located unidirectionally aligned elastic circular fibers (phase 1) with radius a_1, the plane-strain bulk modulus k_1 and the plane-strain shear modulus μ_1, as well as randomly located unidirectionally aligned elastic circular fibers (phase 2) with radius a_2, the plane-strain bulk modulus k_2 and the plane-strain shear modulus μ_2 (cf. Figs. 1, 2). Since the plane-strain is assumed, the fiber interaction exists only in the same cutting plane as shown in Fig. 2. In addition, the plane-strain linearly elastic isotropic stiffness tensors for *three* distinct phases are expressed as

$$\left(C_\eta\right)_{ijkl} = \lambda_\eta \delta_{ij}\delta_{kl} + \mu_\eta \left(\delta_{ik}\delta_{jl} + \delta_{il}\delta_{jk}\right), \quad \eta = 0, 1, 2, \tag{1}$$

where λ_η and μ_η are the Lamé constants of the phase-η material.

Following the eigenstrain concept introduced by Eshelby [21], the perturbed strain field $\boldsymbol{\varepsilon}'(\mathbf{x})$ induced by fibers can be related to the specified eigenstrain $\boldsymbol{\varepsilon}^*(\mathbf{x})$ by replacing the fibers with the matrix material. The

key equation can be rephrased as follows:

$$\mathbf{C}_\eta : \left[\boldsymbol{\varepsilon}^0 + \boldsymbol{\varepsilon}'(\mathbf{x})\right] = \mathbf{C}_0 : \left[\boldsymbol{\varepsilon}^0 + \boldsymbol{\varepsilon}'(\mathbf{x}) - \boldsymbol{\varepsilon}^*(\mathbf{x})\right], \quad \eta = 1, 2, \tag{2}$$

where $\boldsymbol{\varepsilon}^0$ is the uniform strain field induced by the far-field loads for a homogeneous matrix material only. Throughout the paper, the colon symbol ":" denotes the tensor contraction between a fourth-rank tensor and a second-rank tensor, while the dot symbol "•" represents the tensor multiplication between two fourth-rank tensors.

According to Eshelby [21], the perturbed strain induced by the distributed eigenstrain $\boldsymbol{\varepsilon}^*(\mathbf{x})$ in a representative area element (RAE) A reads

$$\boldsymbol{\varepsilon}'(\mathbf{x}) = \int_A \mathbf{G}\left(\mathbf{x} - \mathbf{x}'\right) : \boldsymbol{\varepsilon}^*\left(\mathbf{x}'\right) \mathrm{d}\mathbf{x}', \tag{3}$$

where $\mathbf{x}, \mathbf{x}' \in A$ and the component of the fourth-rank two-dimensional Green's function tensor $\mathbf{G}$ are given by ($i, j, k, l = 1, 2$; cf. Mura [22]):

$$G_{ijkl} = \frac{1}{4\pi\,(1-\nu_0)\,r'^2} F_{ijkl}\,(-8, 2\nu_0, 2, 2-4\nu_0, -1+2\nu_0, 1-2\nu_0), \tag{4}$$

where $\mathbf{r}' \equiv \mathbf{x} - \mathbf{x}'$ and $r' = \left\|\mathbf{r}'\right\|$. The components of the fourth-rank tensor $\mathbf{F}$—which depends on its arguments $(B_1, B_2, B_3, B_4, B_5, B_6)$—are defined by ($m = 1 - 6$):

$$\begin{aligned} F_{ijkl}(B_m) \equiv\; & B_1 n'_i n'_j n'_k n'_l + B_2 \left(\delta_{ik} n'_j n'_l + \delta_{il} n'_j n'_k + \delta_{jk} n'_i n'_l + \delta_{jl} n'_i n'_k\right) + B_3 \delta_{ij} n'_k n'_l \\ & + B_4 \delta_{kl} n'_i n'_j + B_5 \delta_{ij} \delta_{kl} + B_6 \left(\delta_{ik}\delta_{jl} + \delta_{il}\delta_{jk}\right) \end{aligned} \tag{5}$$

with the normal vector $\mathbf{n}' \equiv \mathbf{r}'/r'$. All physical quantities refer to the Cartesian coordinates, and the summation convention applies. Moreover, δ_{ij} denotes the Kronecker delta and ν_0 is the Poisson's ratio of the matrix material. From Eqs. (2) and (3), we arrive at

$$-\mathbf{A}_i : \boldsymbol{\varepsilon}^*(\mathbf{x}) = \boldsymbol{\varepsilon}^0 + \int_A \mathbf{G}\left(\mathbf{x} - \mathbf{x}'\right) : \boldsymbol{\varepsilon}^*\left(\mathbf{x}'\right) \mathrm{d}\mathbf{x}', \quad \mathbf{x} \in A, \tag{6}$$

$$\mathbf{A}_i = \left[\mathbf{C}_i - \mathbf{C}_0\right]^{-1} \bullet \mathbf{C}_0. \tag{7}$$

Within the present two-circular fibers interaction context, the integral equation (6) can be recast as

$$\begin{aligned} & -\mathbf{A}_i : \boldsymbol{\varepsilon}^*_{(i)}(\mathbf{x}) = \boldsymbol{\varepsilon}^0 + \int_{\Omega_i} \mathbf{G}\left(\mathbf{x} - \mathbf{x}'\right) : \boldsymbol{\varepsilon}^*_{(i)}\left(\mathbf{x}'\right)\, \mathrm{d}\mathbf{x}' + \int_{\Omega_j} \mathbf{G}\left(\mathbf{x} - \mathbf{x}'\right) : \boldsymbol{\varepsilon}^*_{(j)}\left(\mathbf{x}'\right) \mathrm{d}\mathbf{x}', \\ & i \neq j, \quad i, j = 1, 2, \end{aligned} \tag{8}$$

where $\mathbf{x} \in \Omega_i$, and $\boldsymbol{\varepsilon}^*_{(i)}(\mathbf{x}')$ is the eigenstrain at $\mathbf{x}'$ in the ith circular fiber within the domain Ω_i.

As discussed earlier in Ju and Chen [25], the first-order solution for the eigenstrain denoted by $\boldsymbol{\varepsilon}^{*0}_{(i)}$ for the i-th phase can be obtained by neglecting the last term in the right-hand side of Eq. (8), which represents the interaction effects due to the other circular fiber. The first-order formulation leads to

$$-\mathbf{A}_i : \boldsymbol{\varepsilon}^{*0}_{(i)} = \boldsymbol{\varepsilon}^0 + \mathbf{S} : \boldsymbol{\varepsilon}^{*0}_{(i)}, \tag{9}$$

where the Eshelby tensor $\mathbf{S}$ is defined as

$$\mathbf{S} = \int_{\Omega_i} \mathbf{G}\left(\mathbf{x} - \mathbf{x}'\right) \mathrm{d}\mathbf{x}', \mathbf{x}, \mathbf{x}' \in \Omega_i. \tag{10}$$

The components of the fourth-rank *interior-point* Eshelby tensor $\mathbf{S}$ for a cylindrical fiber are given by Mura [22], Ju and Sun [38], Sun and Ju [39], and Ju and Zhang [27]. It depends on the Poisson's ratio of the matrix (ν_0) and the shape of the fiber cross-sectional domain Ω_i. In particular, for a two-dimensional circular domain, the components of $\mathbf{S}$ are (see Mura [22] for more details):

$$S_{ijkl} = \frac{1}{8\,(1-\nu_0)} \left[(4\nu_0 - 1)\,\delta_{ij}\delta_{kl} + (3 - 4\nu_0)\left(\delta_{ik}\delta_{jl} + \delta_{il}\delta_{jk}\right)\right], \quad i, j, k, l = 1, 2. \tag{11}$$

By subtracting the first-order solution in Eq. (9) from Eq. (8), the effects of *inter-fiber interaction* can be derived by solving the following integral equation:

$$-\mathbf{A}_i : \mathbf{d}^*_{(i)}(\mathbf{x}) = \int_{\Omega_j} \mathbf{G}\left(\mathbf{x}-\mathbf{x}'\right) \mathrm{d}\mathbf{x}' : \boldsymbol{\varepsilon}^{*0}_{(j)} + \int_{\Omega_i} \mathbf{G}\left(\mathbf{x}-\mathbf{x}'\right) : \mathbf{d}^*_{(i)}\left(\mathbf{x}'\right) \mathrm{d}\mathbf{x}' + \int_{\Omega_j} \mathbf{G}\left(\mathbf{x}-\mathbf{x}'\right) : \mathbf{d}^*_{(j)}\left(\mathbf{x}'\right) \mathrm{d}\mathbf{x}', \quad \text{for} \quad \mathbf{x} \in \Omega_i,\ i \neq j \text{ and } i, j = 1, 2, \tag{12}$$

where

$$\mathbf{d}^*_{(i)}(\mathbf{x}) = \boldsymbol{\varepsilon}^*_{(i)}(\mathbf{x}) - \boldsymbol{\varepsilon}^{*0}_{(i)}. \tag{13}$$

To obtain the *higher-order interaction* correction for $\boldsymbol{\varepsilon}^*_{(i)}(\mathbf{x})$, one may expand the fourth-rank tensor $\mathbf{G}\left(\mathbf{x}-\mathbf{x}'\right)$ in the domain Ω_j with respect to its center point $\mathbf{x}_j$; that is,

$$\mathbf{G}\left(\mathbf{x}-\mathbf{x}'\right) = \mathbf{G}\left(\mathbf{x}-\mathbf{x}_j\right) - \left(\mathbf{x}'-\mathbf{x}_j\right) : \left[\nabla_{\mathbf{x}} \otimes \mathbf{G}\left(\mathbf{x}-\mathbf{x}_j\right)\right] + \frac{1}{2}\left[\left(\mathbf{x}'-\mathbf{x}_j\right) \otimes \left(\mathbf{x}'-\mathbf{x}_j\right)\right] : \left[\nabla_{\mathbf{x}} \otimes \nabla_{\mathbf{x}} \otimes \mathbf{G}\left(\mathbf{x}-\mathbf{x}_j\right)\right] + \cdots \tag{14}$$

where the relation

$$\nabla_{\mathbf{x}'} \otimes \mathbf{G}\left(\mathbf{x}-\mathbf{x}'\right) = -\nabla_{\mathbf{x}} \otimes \mathbf{G}\left(\mathbf{x}-\mathbf{x}'\right) \tag{15}$$

has been employed. From Eqs. (12) and (14), we arrive at

$$\begin{aligned} -\mathbf{A}_i : \mathbf{d}^*_{(i)}(x) = {} & \int_{\Omega_j} \mathbf{G}\left(\mathbf{x}-\mathbf{x}'\right) \mathrm{d}\mathbf{x}' : \boldsymbol{\varepsilon}^{*0}_{(j)} + \int_{\Omega_i} \mathbf{G}\left(\mathbf{x}-\mathbf{x}'\right) : \mathbf{d}^*_{(i)}(\mathbf{x}') \mathrm{d}\mathbf{x}' \\ & + \Omega_j \mathbf{G}\left(\mathbf{x}-\mathbf{x}_j\right) : \bar{\mathbf{d}}^*_{(j)}(\mathbf{x}_j) - \Omega_j a_j \left\{\nabla_{\mathbf{x}} \otimes \mathbf{G}\left(\mathbf{x}-\mathbf{x}_j\right)\right\} : \bar{\mathbf{P}}^*_{(j)} \\ & + \frac{1}{2}\Omega_j a_j^2 \left\{\nabla_{\mathbf{x}} \otimes \nabla_{\mathbf{x}} \otimes \mathbf{G}\left(\mathbf{x}-\mathbf{x}_j\right)\right\} : \bar{\mathbf{Q}}^*_{(j)} + \cdots \end{aligned} \tag{16}$$

for $\mathbf{x} \in \Omega_i$ and $i \neq j$ $(i, j = 1, 2)$. Here $\Omega_i = \pi a_i^2$ and $\Omega_j = \pi a_j^2$ denote the cross-sectional area of a fiber in phase i and j, respectively; a_i and a_j define the fiber radius in phase i and j, respectively. Furthermore, the average fields involved in Eq. (16) are defined as follows:

$$\bar{\mathbf{d}}^*_{(j)} = \frac{1}{\Omega_j} \int_{\Omega_j} \mathbf{d}^*_{(j)}\left(\mathbf{x}'\right) \mathrm{d}\mathbf{x}'; \bar{\mathbf{P}}^*_{(j)} = \frac{1}{\Omega_j a_j} \int_{\Omega_j} \left(\mathbf{x}'-\mathbf{x}_j\right) \otimes \mathbf{d}^*_{(j)}\left(\mathbf{x}'\right) \mathrm{d}\mathbf{x}', \tag{17}$$

$$\bar{\mathbf{Q}}^*_{(j)} = \frac{1}{\Omega_j a_j^2} \int_{\Omega_j} \left(\mathbf{x}'-\mathbf{x}_j\right) \otimes \left(\mathbf{x}'-\mathbf{x}_j\right) \otimes \mathbf{d}^*_{(j)}\left(\mathbf{x}'\right) \mathrm{d}\mathbf{x}'. \tag{18}$$

The third-rank tensor $\bar{\mathbf{P}}^*_{(j)}$ and the fourth-rank tensor $\bar{\mathbf{Q}}^*_{(j)}$ correspond to the dipole and quadrupole of $\bar{\mathbf{d}}^*_{(j)}$ in the domain Ω_j, respectively. Due to the circular symmetry of fibers, the leading order of $\bar{\mathbf{P}}^*_{(j)}$ can be shown to be of the order $O\left(\rho_j^3\right)$, rather than $O\left(\rho_j^2\right)$, by substituting Eq. (16) into Eq. (17). Here, $\rho_j = a_j/r$ and r is the spacing between the centers of two interacting fibers. By performing the *area average* of Eq. (16) for the domain Ω_i and neglecting those terms of higher-order moments in Eq. (16), the *approximate* equations for $\bar{\mathbf{d}}^*_{(j)}$ for the local *two-fiber interaction* problem can be obtained. Letting $i = 1$, $j = 2$, Eqs. (19)–(22) are derived. In addition, letting $i = 2$, $j = 1$, Eqs. (23)–(26) are obtained.

$$-\mathbf{A}_1 : \Omega_1 \bar{\mathbf{d}}^*_{(1)} = \Omega_{12} \bar{\mathbf{G}}^{21} : \boldsymbol{\varepsilon}^{*0}_{(2)} + \Omega_1 \mathbf{S} : \bar{\mathbf{d}}^*_{(1)} + \Omega_2 \bar{\mathbf{G}}^{11} : \bar{\mathbf{d}}^*_{(2)} + O\left(\rho^6\right), \tag{19}$$

where

$$\bar{\mathbf{d}}^*_{(1)} = \frac{1}{\Omega_1}\int\limits_{\Omega_1} \mathbf{d}^*_{(1)}\left(\mathbf{x}'\right)\mathrm{d}\mathbf{x}';\quad \mathbf{S} = \int\limits_{\Omega_1} \mathbf{G}(\mathbf{x}-\mathbf{x}')\,\mathrm{d}\mathbf{x}'\ (\mathbf{x}\in\Omega_1;\mathbf{x}'\in\Omega_1), \tag{20}$$

$$\bar{\mathbf{G}}^{21} = \frac{1}{\Omega_{12}}\int\limits_{\Omega_1}\int\limits_{\Omega_2} \mathbf{G}(\mathbf{x}-\mathbf{x}')\mathrm{d}\mathbf{x}'\mathrm{d}\mathbf{x} = \frac{1}{8\,(1-\nu_0)}\left[\rho_1\rho_2\mathbf{H}^1 + \left(\frac{\rho_1^3\rho_2+\rho_1\rho_2^3}{2}\right)\mathbf{H}^2\right], \tag{21}$$

$$\bar{\mathbf{G}}^{11} = \int\limits_{\Omega_1} \mathbf{G}(\mathbf{x}-\mathbf{x}_2)\,\mathrm{d}\mathbf{x} = \frac{1}{8\,(1-\nu_0)}\left(\rho_1^2\mathbf{H}^1 + \frac{\rho_1^4}{2}\mathbf{H}^2\right),\quad \text{with } \mathbf{x}\in\Omega_1, \mathbf{x}_2\in\Omega_2. \tag{22}$$

In addition, we have

$$-\mathbf{A}_2 : \Omega_2\,\bar{\mathbf{d}}^*_{(2)} = \Omega_{21}\,\bar{\mathbf{G}}^{12} : \boldsymbol{\varepsilon}^{*0}_{(1)} + \Omega_2\,\mathbf{S}\ : \bar{\mathbf{d}}^*_{(2)} + \Omega_1\,\bar{\mathbf{G}}^{22} : \bar{\mathbf{d}}^*_{(1)} + O\left(\rho^6\right) \tag{23}$$

in which

$$\bar{\mathbf{d}}^*_{(2)} = \frac{1}{\Omega_2}\int\limits_{\Omega_2} \mathbf{d}^*_{(2)}\left(\mathbf{x}'\right)\mathrm{d}\mathbf{x}'\,;\mathbf{S} = \int\limits_{\Omega_2} \mathbf{G}(\mathbf{x}-\mathbf{x}')\mathrm{d}\mathbf{x}'\quad (\mathbf{x}\in\Omega_2;\mathbf{x}'\in\Omega_2), \tag{24}$$

$$\bar{\mathbf{G}}^{12} = \frac{1}{\Omega_{21}}\int\limits_{\Omega_2}\int\limits_{\Omega_1} \mathbf{G}(\mathbf{x}-\mathbf{x}')\,\mathrm{d}\mathbf{x}'\mathrm{d}\mathbf{x} = \frac{1}{8\,(1-\nu_0)}\left[\rho_1\rho_2\mathbf{H}^1 + \left(\frac{\rho_1^3\rho_2+\rho_1\rho_2^3}{2}\right)\mathbf{H}^2\right], \tag{25}$$

$$\bar{\mathbf{G}}^{22} = \int\limits_{\Omega_2} \mathbf{G}(\mathbf{x}-\mathbf{x}_1)\,\mathrm{d}\mathbf{x} = \frac{1}{8\,(1-\nu_0)}\left(\rho_2^2\mathbf{H}^1 + \frac{\rho_2^4}{2}\mathbf{H}^2\right),\quad \text{with } \mathbf{x}\in\Omega_2, \mathbf{x}_1\in\Omega_1 \tag{26}$$

and the components of $\mathbf{H}^1$ and $\mathbf{H}^2$are rendered by

$$\begin{aligned} H^1_{ijkl}\left(\mathbf{x}_1-\mathbf{x}_2\right) &\equiv 2F_{ijkl}\left(-8, 2\nu_0, 2, 2-4\nu_0, -1+2\nu_0, 1-2\nu_0\right),\\ H^2_{ijkl}\left(\mathbf{x}_1-\mathbf{x}_2\right) &\equiv 2F_{ijkl}\left(24, -4, -4, -4, 1,\ 1\right). \end{aligned} \tag{27}$$

Moreover, we define $\rho_1 = a_1/r$, $\rho_2 = a_2/r$, $\Omega_{12} = \pi a_1 a_2$ and $\Omega_{21} = \Omega_{12} = \pi a_1\, a_2$.

It is interesting to note that $\bar{\mathbf{G}}^{11}$ in Eq. (22) and $\bar{\mathbf{G}}^{22}$ in Eq. (26) are different from the Eshelby tensor $\mathbf{S}$ in Eq. (20) and in Eq. (24). One may refer to $\bar{\mathbf{G}}^{11}$ and $\bar{\mathbf{G}}^{22}$ as the "*exterior-point* Eshelby tensors" since the integrals in Eqs. (22) and (26) involve an *exterior-point* outside the integration domain. It should be noted that the leading order induced by truncating the higher-order moments in Eqs. (19) and (23) is of the order $O\left(\rho^6\right)$, since both $\bar{\mathbf{P}}^*_{(j)}$ and $\Omega_j a_j\left\{\nabla_x\otimes\mathbf{G}\left(\mathbf{x}-\mathbf{x}_j\right)\right\}$ are of the order $O\left(\rho^3\right)$. Moreover, Eqs. (19) and (23) can be recast as

$$\begin{aligned} \Omega_1\left(\mathbf{A}_1+\mathbf{S}\right) : \bar{\mathbf{d}}^*_{(1)} + \Omega_2\,\bar{\mathbf{G}}^{11} : \bar{\mathbf{d}}^*_{(2)} &= -\Omega_{12}\,\bar{\mathbf{G}}^{21} : \boldsymbol{\varepsilon}^{*0}_{(2)},\\ \Omega_1\,\bar{\mathbf{G}}^{22} : \bar{\mathbf{d}}^*_{(1)} + \Omega_2\left(\mathbf{A}_2+\mathbf{S}\right) : \bar{\mathbf{d}}^*_{(2)} &= -\Omega_{12}\,\bar{\mathbf{G}}^{12} : \boldsymbol{\varepsilon}^{*0}_{(1)}. \end{aligned} \tag{28}$$

Therefore, the solutions of Eq. (28) are

$$\begin{aligned} \bar{\mathbf{d}}^*_{(1)} = \frac{\Omega_{12}}{\Omega_1}&\left[\left(\bar{\mathbf{G}}^{11}\right)^{-1}\bullet\left(\mathbf{A}_1+\mathbf{S}\right) - \bar{\mathbf{G}}^{22}\bullet\left(\mathbf{A}_2+\mathbf{S}\right)^{-1}\right]^{-1}\\ &\bullet\left[\left(\mathbf{A}_2+\mathbf{S}\right)^{-1}\bullet\bar{\mathbf{G}}^{12} : \boldsymbol{\varepsilon}^{*0}_{(1)} - \left(\bar{\mathbf{G}}^{11}\right)^{-1}\bullet\bar{\mathbf{G}}^{21} : \boldsymbol{\varepsilon}^{*0}_{(2)}\right], \end{aligned} \tag{29}$$

$$\begin{aligned} \bar{\mathbf{d}}^*_{(2)} = \frac{\Omega_{12}}{\Omega_2}&\left[\bar{\mathbf{G}}^{11}\bullet\left(\mathbf{A}_1+\mathbf{S}\right)^{-1} - \left(\bar{\mathbf{G}}^{22}\right)^{-1}\bullet\left(\mathbf{A}_2+\mathbf{S}\right)\right]^{-1}\\ &\bullet\left[\left(\bar{\mathbf{G}}^{22}\right)^{-1}\bullet\bar{\mathbf{G}}^{12} : \boldsymbol{\varepsilon}^{*0}_{(1)} - \bar{\mathbf{G}}^{21}\bullet\left(\mathbf{A}_1+\mathbf{S}\right)^{-1} : \boldsymbol{\varepsilon}^{*0}_{(2)}\right], \end{aligned} \tag{30}$$

where the leading orders of $\bar{\mathbf{G}}^{22}\,(\mathbf{A}_2+\mathbf{S})^{-1}$ and $\left(\bar{\mathbf{G}}^{11}\right)^{-1}(\mathbf{A}_1+\mathbf{S})$ are of the order of $O\left(\rho^2\right)$ and $O\left(\rho^{-2}\right)$ in Eq. (29), respectively. We note that $\bar{\mathbf{G}}^{22}\,(\mathbf{A}_2+\mathbf{S})^{-1}$ is truncated since its leading order is greater than the leading order of $\left(\bar{\mathbf{G}}^{11}\right)^{-1}(\mathbf{A}_1+\mathbf{S})$. We also have $\rho_1 \leq 1/2$, $\rho_2 \leq 1/2$, and $\rho_1+\rho_2 \leq 1$:

$$\mathbf{d}^*_{(1)} = \frac{\Omega_{12}}{\Omega_1}\left[(\mathbf{A}_1+\mathbf{S})^{-1} \bullet \bar{\mathbf{G}}^{11} \bullet (\mathbf{A}_2+\mathbf{S})^{-1} \bullet \bar{\mathbf{G}}^{12} : \boldsymbol{\varepsilon}^{*0}_{(1)} - (\mathbf{A}_1+\mathbf{S})^{-1} \bullet \bar{\mathbf{G}}^{21} : \boldsymbol{\varepsilon}^{*0}_{(2)}\right]. \tag{31}$$

Similarly, Eq. (30) can be rephrased as

$$\bar{\mathbf{d}}^*_{(2)} = \frac{\Omega_{12}}{\Omega_2}\left[(\mathbf{A}_2+\mathbf{S})^{-1} \bullet \bar{\mathbf{G}}^{22} \bullet (\mathbf{A}_1+\mathbf{S})^{-1} \bullet \bar{\mathbf{G}}^{21} : \boldsymbol{\varepsilon}^{*0}_{(2)} - (\mathbf{A}_2+\mathbf{S})^{-1} \bullet \bar{\mathbf{G}}^{12} : \boldsymbol{\varepsilon}^{*0}_{(1)}\right]. \tag{32}$$

3 Ensemble-area averaged eigenstrains

To obtain the probabilistic ensemble averaged solution of $\bar{\mathbf{d}}^*_{(1)}$ within the context of approximate pairwise local fiber interaction, one has to integrate Eq. (31) over all possible positions $(\mathbf{x}_2)$ of the phase-2 fiber and positions $(\mathbf{x}_1)$ of the phase-1 fiber for a given location of the phase-1 fiber $(\mathbf{x}_1)$. Similarly, to find $\bar{\mathbf{d}}^*_{(2)}$, one has to integrate Eq. (32) over all possible positions $(\mathbf{x}_1)$ of the phase-1 fiber and positions $(\mathbf{x}_2)$ of the phase-2 fiber for a given location of the phase-2 fiber$(\mathbf{x}_2)$. The ensemble average process takes the form

$$\left\langle \bar{\mathbf{d}}^*_{(i)} \right\rangle (\mathbf{x}_i) = \int\limits_{A-\Omega_i} \bar{\mathbf{d}}^*_{(i)}\left(\mathbf{x}_i - \mathbf{x}_j\right) P\left(\mathbf{x}_j \middle| \mathbf{x}_i\right) \mathrm{d}\mathbf{x}_j, \qquad i \neq j, \tag{33}$$

$$i=1,\, j=2: \quad \left\langle \bar{\mathbf{d}}^*_{(1)} \right\rangle (\mathbf{x}_1) = \int\limits_{A-\Omega_1} \bar{\mathbf{d}}^*_{(1)}\left(\mathbf{x}_1 - \mathbf{x}_2\right) P\left(\mathbf{x}_2 \middle| \mathbf{x}_1\right) \mathrm{d}\mathbf{x}_2, \tag{34}$$

$$i=2,\, j=1: \quad \left\langle \bar{\mathbf{d}}^*_{(2)} \right\rangle (\mathbf{x}_2) = \int\limits_{A-\Omega_2} \bar{\mathbf{d}}^*_{(2)}\left(\mathbf{x}_2 - \mathbf{x}_1\right) P\left(\mathbf{x}_1 \middle| \mathbf{x}_2\right) \mathrm{d}\mathbf{x}_1. \tag{35}$$

The two-point conditional probability function $P\left(\mathbf{x}_j \middle| \mathbf{x}_i\right)$ is determined by the microstructure of a composite, which in turn depends on the fiber volume fractions and underlying manufacturing processes. For illustration, the two-point conditional probability density function is taken in the following form:

$$P\left(\mathbf{x}_j \middle| \mathbf{x}_i\right) = \begin{cases} \frac{(N_i+N_j)}{A}\, g\left(\widehat{r}\right), & \text{if } \widehat{r} \geq 1\,, \quad \text{where } \widehat{r} \equiv r/(a_1+a_2)\,, \quad r > (a_1+a_2)\,, \\ 0, & \text{otherwise,} \end{cases} \tag{36}$$

where $i,\, j = 1, 2,\, i \neq j$; N_i and N_i/A are the numbers of fibers and the 2-D number density of fibers in phase i in a composite, respectively; N_j and N_j/A are the numbers of fibers and 2-D number density of fibers in phase j (*distinct* material property and size of phase i) in a composite, respectively; r is the spacing between centers of two fibers. Further, $g\left(\widehat{r}\right)$ denotes the 2-D transversely isotropic "radial distribution function" (Hansen and McDonald [57]; Torquato and Lado [14]).

By substituting Eq. (31) into (34), the explicit expression for $\left\langle \bar{\mathbf{d}}^*_{(1)} \right\rangle (\mathbf{x}_1)$ can be depicted as

$$\begin{aligned} \left\langle \bar{\mathbf{d}}^*_{(1)} \right\rangle (\mathbf{x}_1) &= \int\limits_{A-\Omega_1} \bar{\mathbf{d}}^*_{(1)}\left(\mathbf{x}_1 - \mathbf{x}_2\right) P\left(\mathbf{x}_2 \middle| \mathbf{x}_1\right) \mathrm{d}\mathbf{x}_2 \\ &= \int\limits_{A-\Omega_1} \frac{\Omega_{12}}{\Omega_1}\left[(\mathbf{A}_1+\mathbf{S})^{-1}\,\bar{\mathbf{G}}^{11}\,(\mathbf{A}_2+\mathbf{S})^{-1}\,\bar{\mathbf{G}}^{12} : \boldsymbol{\varepsilon}^{*0}_{(1)} - (\mathbf{A}_1+\mathbf{S})^{-1}\,\bar{\mathbf{G}}^{21} : \boldsymbol{\varepsilon}^{*0}_{(2)}\right] P\left(\mathbf{x}_2 \middle| \mathbf{x}_1\right) \mathrm{d}\mathbf{x}_2 \end{aligned}$$

$$= \frac{\Omega_{12}}{\Omega_1} \int\limits_{a_1+a_2}^{\infty} \int\limits_{0}^{2\pi} \left[(\mathbf{A}_1 + \mathbf{S})^{-1} \bar{\mathbf{G}}^{11} (\mathbf{A}_2 + \mathbf{S})^{-1} \bar{\mathbf{G}}^{12} : \boldsymbol{\varepsilon}^{*0}_{(1)} \right] P(\mathbf{x}_2 | \mathbf{x}_1) \, \mathrm{d}\mathbf{x}_2$$

$$+ \frac{\Omega_{12}}{\Omega_1} \int\limits_{2a_1}^{\infty} \int\limits_{0}^{2\pi} \left[(\mathbf{A}_1 + \mathbf{S})^{-1} \bar{\mathbf{G}}^{11} (\mathbf{A}_2 + \mathbf{S})^{-1} \bar{\mathbf{G}}^{12} : \boldsymbol{\varepsilon}^{*0}_{(1)} \right] P(\mathbf{x}_1 | \mathbf{x}_1) \, \mathrm{d}\mathbf{x}_1. \tag{37}$$

Here, we can prove that

$$\int\limits_{A-\Omega_1} \frac{\Omega_{12}}{\Omega_1} \left[(\mathbf{A}_1 + \mathbf{S})^{-1} \bar{\mathbf{G}}^{21} : \boldsymbol{\varepsilon}^{*0}_{(2)} \right] P(\mathbf{x}_2 | \mathbf{x}_1) \, \mathrm{d}\mathbf{x}_2 = 0, \tag{38}$$

where $\int_0^{2\pi} \mathbf{H}^1(\mathbf{n}) \, \mathrm{d}\theta = 0$; $\int_0^{2\pi} \mathbf{H}^2(\mathbf{n}) \, \mathrm{d}\theta = 0$ as shown in Ju and Zhang [27]; A is the infinitely large 2-D transversely isotropic *probabilistic* (not physical) integration domain; $\Omega_1$is probabilistic "exclusion zone" for $\mathbf{x}_2$. In addition, the following identities can be easily derived:

$$\int\limits_0^{2\pi} n_i n_j \mathrm{d}\theta = \pi \delta_{ij}; \int\limits_0^{2\pi} n_i n_j n_k n_l \mathrm{d}\theta = \frac{\pi}{4} \left(\delta_{ij}\delta_{kl} + \delta_{ik}\delta_{jl} + \delta_{il}\delta_{jk} \right). \tag{39}$$

Similarly, by substituting Eq. (32) into Eq. (35), the explicit expression for $\left\langle \bar{\mathbf{d}}^{*}_{(2)} \right\rangle (\mathbf{x}_2)$ can be expressed as

$$\left\langle \bar{\mathbf{d}}^{*}_{(2)} \right\rangle (\mathbf{x}_2) = \int\limits_{A-\Omega_2} \bar{\mathbf{d}}^{*}_{(2)} (\mathbf{x}_2 - \mathbf{x}_1) \, P(\mathbf{x}_1 | \mathbf{x}_2) \, \mathrm{d}\mathbf{x}_1$$

$$= \int\limits_{A-\Omega_2} \frac{\Omega_{12}}{\Omega_2} \left[(\mathbf{A}_2 + \mathbf{S})^{-1} \bar{\mathbf{G}}^{22} (\mathbf{A}_1 + \mathbf{S})^{-1} \bar{\mathbf{G}}^{21} : \boldsymbol{\varepsilon}^{*0}_{(2)} - (\mathbf{A}_2 + \mathbf{S})^{-1} \bar{\mathbf{G}}^{12} : \boldsymbol{\varepsilon}^{*0}_{(1)} \right] P(\mathbf{x}_1 | \mathbf{x}_2) \, \mathrm{d}\mathbf{x}_1$$

$$= \frac{\Omega_{12}}{\Omega_2} \int\limits_{a_1+a_2}^{\infty} \int\limits_{0}^{2\pi} \left[(\mathbf{A}_2 + \mathbf{S})^{-1} \bar{\mathbf{G}}^{22} (\mathbf{A}_1 + \mathbf{S})^{-1} \bar{\mathbf{G}}^{21} : \boldsymbol{\varepsilon}^{*0}_{(2)} \right] P(\mathbf{x}_1 | \mathbf{x}_2) \, \mathrm{d}\mathbf{x}_1$$

$$+ \frac{\Omega_{12}}{\Omega_2} \int\limits_{2a_2}^{\infty} \int\limits_{0}^{2\pi} \left[(\mathbf{A}_2 + \mathbf{S})^{-1} \bar{\mathbf{G}}^{22} (\mathbf{A}_1 + \mathbf{S})^{-1} \bar{\mathbf{G}}^{21} : \boldsymbol{\varepsilon}^{*0}_{(2)} \right] P(\mathbf{x}_2 | \mathbf{x}_2) \, \mathrm{d}\mathbf{x}_2. \tag{40}$$

Here, we can also prove that

$$\int\limits_{A-\Omega_2} \frac{\Omega_{12}}{\Omega_2} \left[(\mathbf{A}_2 + \mathbf{S})^{-1} \bar{\mathbf{G}}^{12} : \boldsymbol{\varepsilon}^{*0}_{(1)} \right] P(\mathbf{x}_1 | \mathbf{x}_2) \, \mathrm{d}\mathbf{x}_1 = 0. \tag{41}$$

In what follows, two different radial distribution functions will be considered; that is, (1) the *uniform* radial distribution function $g\left(\hat{r}\right) = 1$ and (2) the *general* radial distribution function $g\left(\hat{r}\right) \neq 1$ in Eq. (36). Under each radial distribution function, we present two non-equivalent formulations to predict the effective transverse elastic moduli of two-phase composites; that is, "Formulation II" and "Formulation I." The following notations are adopted: the superscript "U", "G", "II", and "I" stand for the *uniform* radial distribution function, the *general* radial distribution function, Formulation II and Formulation I, respectively.

3.1 Radial distribution function (URDF): $g\left(\hat{r}\right) = 1$

This event corresponds to the simplest approximation for $g\left(\hat{r}\right)$ since it tends to underestimate the probability of the surrounding fibers at high fiber volume fraction during the ensemble-area averaging process. Therefore, this case may be regarded as the "lower bound" for microstructure and is more suitable for low fiber concentrations.

Formulation II: By carrying out lengthy algebra and utilizing identities Eqs. (17), (36) and (39), the approximate ensemble-area averaged eigenstrain tensor $\left\langle \bar{\boldsymbol{\varepsilon}}^{*}_{(1)} \right\rangle$ can be derived as follows

$$\left\langle \bar{\boldsymbol{\varepsilon}}^{*}_{(1)} \right\rangle^{\mathrm{UII}} = \underset{\sim}{\boldsymbol{\Gamma}}^{\mathrm{UII}}_{(1)} : \boldsymbol{\varepsilon}^{*0}_{(1)}. \tag{42}$$

Here, the components of the isotropic tensor $\underset{\sim}{\boldsymbol{\Gamma}}^{\mathrm{UII}}_{(1)}$ are:

$$\underset{\sim}{\boldsymbol{\Gamma}}^{\mathrm{UII}}_{(1)} = \gamma^{\mathrm{UII}}_{11}\delta_{ij}\delta_{kl} + \gamma^{\mathrm{UII}}_{21}\left(\delta_{ik}\delta_{jl} + \delta_{il}\delta_{jk}\right), \tag{43}$$

$$\gamma^{\mathrm{UII}}_{11} = \frac{\phi^{(2)}}{4}\mathbf{U}^{\mathrm{UII}}_{21} + \frac{\phi^{(1)}}{4}\mathbf{U}^{\mathrm{UII}}_{11}; \quad \gamma^{\mathrm{UII}}_{21} = \frac{1}{2} + \frac{\phi^{(2)}}{4}\mathbf{V}^{\mathrm{UII}}_{21} + \frac{\phi^{(1)}}{4}\mathbf{V}^{\mathrm{UII}}_{11}, \tag{44}$$

$$\mathbf{U}^{\mathrm{UII}}_{21} = f^{\mathrm{U}}_{11} + \frac{6}{\beta_1\beta_2}\left[\frac{\lambda^2+2\lambda^4}{(1+\lambda)^4} - \frac{\lambda^4+\lambda^6}{(1+\lambda)^6}\right]; \qquad \mathbf{U}^{\mathrm{UII}}_{11} = t^{\mathrm{U}}_{11} + \frac{15}{16\beta_1^2}, \tag{45}$$

$$\mathbf{V}^{\mathrm{UII}}_{21} = f^{\mathrm{U}}_{21} - \frac{6}{\beta_1\beta_2}\left[\frac{\lambda^2+2\lambda^4}{(1+\lambda)^4} - \frac{\lambda^4+\lambda^6}{(1+\lambda)^6}\right]; \qquad \mathbf{V}^{\mathrm{UII}}_{11} = t^{\mathrm{U}}_{21} - \frac{15}{16\beta_1^2}, \tag{46}$$

$$\begin{aligned} &\lambda = \frac{a_1}{a_2}; \qquad \beta_1 = 4\left(1-\nu_0\right)\frac{\mu_0}{\mu_1-\mu_0} + \left(3-4\nu_0\right), \\ &\beta_2 = 4\left(1-\nu_0\right)\frac{\mu_0}{\mu_2-\mu_0} + \left(3-4\nu_0\right), \end{aligned} \tag{47}$$

where $\phi^{(2)}$ and $\phi^{(1)}$ are the fiber volume fractions of phase 2 and phase 1, respectively. Similarly, the approximate ensemble-area averaged eigenstrain tensor $\left\langle \bar{\boldsymbol{\varepsilon}}^{*}_{(2)} \right\rangle$ is

$$\left\langle \bar{\boldsymbol{\varepsilon}}^{*}_{(2)} \right\rangle^{\mathrm{UII}} = \underset{\sim}{\boldsymbol{\Gamma}}^{\mathrm{UII}}_{(2)} : \boldsymbol{\varepsilon}^{*0}_{(2)}. \tag{48}$$

Here, the components of the isotropic tensor $\underset{\sim}{\boldsymbol{\Gamma}}^{\mathrm{UII}}_{(2)}$ read:

$$\underset{\sim}{\Gamma}^{\mathrm{UII}}_{(2)} = \gamma^{\mathrm{UII}}_{12}\delta_{ij}\delta_{kl} + \gamma^{\mathrm{UII}}_{22}\left(\delta_{ik}\delta_{jl} + \delta_{il}\delta_{jk}\right), \tag{49}$$

$$\gamma^{\mathrm{UII}}_{12} = \frac{\phi^{(1)}}{4}\mathbf{U}^{\mathrm{UII}}_{12} + \frac{\phi^{(2)}}{4}\mathbf{U}^{\mathrm{UII}}_{22}; \quad \gamma^{\mathrm{UII}}_{22} = \frac{1}{2} + \frac{\phi^{(1)}}{4}\mathbf{V}^{\mathrm{UII}}_{12} + \frac{\phi^{(2)}}{4}\mathbf{V}^{\mathrm{UII}}_{22}, \tag{50}$$

$$\mathbf{U}^{\mathrm{UII}}_{12} = f^{\mathrm{U}}_{12} + \frac{6}{\beta_1\beta_2}\left[\frac{\eta^2+2\eta^4}{(1+\eta)^4} - \frac{\eta^4+\eta^6}{(1+\eta)^6}\right]; \quad \mathbf{U}^{\mathrm{UII}}_{22} = t^{\mathrm{U}}_{12} + \frac{15}{16\beta_2^2}, \tag{51}$$

$$\mathbf{V}^{\mathrm{UII}}_{12} = f^{\mathrm{U}}_{22} - \frac{6}{\beta_1\beta_2}\left[\frac{\eta^2+2\eta^4}{(1+\eta)^4} - \frac{\eta^4+\eta^6}{(1+\eta)^6}\right]; \quad \mathbf{V}^{\mathrm{UII}}_{22} = t^{\mathrm{U}}_{22} - \frac{15}{16\beta_2^2}, \tag{52}$$

$$\begin{aligned} &\eta = \frac{a_2}{a_1} = \frac{1}{\lambda}; \quad \beta_1 = 4\left(1-\nu_0\right)\frac{\mu_0}{\mu_1-\mu_0} + \left(3-4\nu_0\right), \\ &\beta_2 = 4\left(1-\nu_0\right)\frac{\mu_0}{\mu_2-\mu_0} + \left(3-4\nu_0\right). \end{aligned} \tag{53}$$

Formulation I: By neglecting the higher-order components $O\left(\rho_1^4/2\right)$ associated with $\mathbf{H}^2$ in Eq. (22), $O\left(\rho_2^4/2\right)$ associated with $\mathbf{H}^2$ in Eq. (26), and $O\left(\frac{\rho_1^3\rho_2+\rho_1\rho_2^3}{2}\right)$ associated with $\mathbf{H}^2$ in Eq. (25) and following similar procedures as in "Formulation II", the approximate ensemble-area averaged eigenstrain tensor $\left\langle \bar{\boldsymbol{\varepsilon}}^{*}_{(1)} \right\rangle$ becomes

$$\left\langle \bar{\boldsymbol{\varepsilon}}^{*}_{(1)} \right\rangle^{\mathrm{UI}} = \underset{\sim}{\boldsymbol{\Gamma}}^{\mathrm{UI}}_{(1)} : \boldsymbol{\varepsilon}^{*0}_{(1)}. \tag{54}$$

Here, the components of the isotropic tensor $\underset{\sim}{\mathbf{\Gamma}}^{\mathrm{UI}}_{(1)}$ are:

$$\underset{\sim}{\mathbf{\Gamma}}^{\mathrm{UI}}_{(1)} = \gamma^{\mathrm{UI}}_{11}\delta_{ij}\delta_{kl} + \gamma^{\mathrm{UI}}_{21}\left(\delta_{ik}\delta_{jl} + \delta_{il}\delta_{jk}\right), \tag{55}$$

$$\gamma^{\mathrm{UI}}_{11} = \frac{\phi^{(2)}}{4}\mathbf{U}^{\mathrm{UI}}_{21} + \frac{\phi^{(1)}}{4}\mathbf{U}^{\mathrm{UI}}_{11}; \quad \gamma^{\mathrm{UI}}_{21} = \frac{1}{2} + \frac{\phi^{(2)}}{4}\mathbf{V}^{\mathrm{UI}}_{21} + \frac{\phi^{(1)}}{4}\mathbf{V}^{\mathrm{UI}}_{11}, \tag{56}$$

$$\mathbf{U}^{\mathrm{UI}}_{21} = f^{\mathrm{U}}_{11}; \quad \mathbf{U}^{\mathrm{UI}}_{11} = t^{\mathrm{U}}_{11}; \quad \mathbf{V}^{\mathrm{UI}}_{21} = f^{\mathrm{U}}_{21}; \quad \mathbf{V}^{\mathrm{UI}}_{11} = t^{\mathrm{U}}_{21}, \tag{57}$$

$$\begin{aligned} f^{\mathrm{U}}_{11} &= \frac{-4\lambda^2}{(1+\lambda)^2}\frac{\{\alpha_1\left[2\alpha_2 + (3-2\nu_0)\,\beta_2\right] + \beta_1\left[4\nu_0\alpha_2 + (2\nu_0+1)\,\beta_2\right]\}}{\beta_1\beta_2\,(\alpha_1+\beta_1)\,(\alpha_2+\beta_2)}, \\ t^{\mathrm{U}}_{11} &= \frac{1}{\beta_1^2}\left[-2 + \frac{(1-2\nu_0)\,\beta_1}{\alpha_1+\beta_1}\right]; \quad f^{\mathrm{U}}_{21} = \frac{4\lambda^2}{(1+\lambda)^2}\frac{(2\alpha_2 + 3\beta_2 - 2\nu_0\beta_2)}{\beta_1\beta_2\,(\alpha_2+\beta_2)}, \end{aligned} \tag{58}$$

$$\begin{aligned} t^{\mathrm{U}}_{21} &= \frac{1}{\beta_1^2}\left[2 + \frac{(1-2\nu_0)\,\beta_1}{\alpha_1+\beta_1}\right]; \quad \alpha_1 = 4\,(1-\nu_0)\left[\frac{k_0}{k_1-k_0} - \frac{\mu_0}{\mu_1-\mu_0}\right] + (4\nu_0 - 1)\,, \\ \alpha_2 &= 4\,(1-\nu_0)\left[\frac{k_0}{k_2-k_0} - \frac{\mu_0}{\mu_2-\mu_0}\right] + (4\nu_0 - 1)\,. \end{aligned} \tag{59}$$

Similarly, the approximate ensemble-area averaged eigenstrain tensor $\left\langle \bar{\boldsymbol{\varepsilon}}^{*}_{(2)} \right\rangle$ is

$$\left\langle \bar{\boldsymbol{\varepsilon}}^{*}_{(2)} \right\rangle^{\mathrm{UI}} = \underset{\sim}{\mathbf{\Gamma}}^{\mathrm{UI}}_{(2)} : \boldsymbol{\varepsilon}^{*0}_{(2)}. \tag{60}$$

Here, the components of the isotropic tensor $\underset{\sim}{\Gamma}^{\mathrm{UI}}_{(2)}$ are:

$$\underset{\sim}{\mathbf{\Gamma}}^{\mathrm{UI}}_{(2)} = \gamma^{\mathrm{UI}}_{12}\delta_{ij}\delta_{kl} + \gamma^{\mathrm{UI}}_{22}\left(\delta_{ik}\delta_{jl} + \delta_{il}\delta_{jk}\right), \tag{61}$$

$$\gamma^{\mathrm{UI}}_{12} = \frac{\phi^{(1)}}{4}\mathbf{U}^{\mathrm{UI}}_{12} + \frac{\phi^{(2)}}{4}\mathbf{U}^{\mathrm{UI}}_{22}; \quad \gamma^{\mathrm{UI}}_{22} = \frac{1}{2} + \frac{\phi^{(1)}}{4}\mathbf{V}^{\mathrm{UI}}_{12} + \frac{\phi^{(2)}}{4}\mathbf{V}^{\mathrm{UI}}_{22}, \tag{62}$$

$$\mathbf{U}^{\mathrm{UI}}_{12} = f^{\mathrm{U}}_{12}; \quad \mathbf{U}^{\mathrm{UI}}_{22} = t^{\mathrm{U}}_{12}; \quad \mathbf{V}^{\mathrm{UI}}_{12} = f^{\mathrm{U}}_{22}; \quad \mathbf{V}^{\mathrm{UI}}_{22} = t^{\mathrm{U}}_{22}, \tag{63}$$

$$\begin{aligned} f^{\mathrm{U}}_{12} &= \frac{-4\eta^2}{(1+\eta)^2}\frac{\{\alpha_2\left[2\alpha_1 + (3-2\nu_0)\,\beta_1\right] + \beta_2\left[4\nu_0\alpha_1 + (2\nu_0+1)\,\beta_1\right]\}}{\beta_1\beta_2\,(\alpha_1+\beta_1)\,(\alpha_2+\beta_2)}, \\ t^{\mathrm{U}}_{12} &= \frac{1}{\beta_2^2}\left[-2 + \frac{(1-2\nu_0)\,\beta_2}{\alpha_2+\beta_2}\right]; \quad f^{\mathrm{U}}_{22} = \frac{4\eta^2}{(1+\eta)^2}\frac{(2\alpha_1 + 3\beta_1 - 2\nu_0\beta_1)}{\beta_1\beta_2\,(\alpha_1+\beta_1)}, \end{aligned} \tag{64}$$

$$\begin{aligned} t^{\mathrm{U}}_{22} &= \frac{1}{\beta_2^2}\left[2 + \frac{(1-2\nu_0)\,\beta_2}{\alpha_2+\beta_2}\right]; \qquad \alpha_1 = 4\,(1-\nu_0)\left[\frac{k_0}{k_1-k_0} - \frac{\mu_0}{\mu_1-\mu_0}\right] + (4\nu_0 - 1)\,, \\ \alpha_2 &= 4\,(1-\nu_0)\left[\frac{k_0}{k_2-k_0} - \frac{\mu_0}{\mu_2-\mu_0}\right] + (4\nu_0 - 1)\,. \end{aligned} \tag{65}$$

3.2 General radial distribution function (GRDF): $g\left(\widehat{r}\right) \neq 1$

This event corresponds to the complex approximation for $g\left(\widehat{r}\right)$ since it tends to overestimate the probability of the surrounding fibers at low fiber volume fraction during the ensemble-area averaging process. Therefore, this case may be regarded as the "upper bound" for microstructure and is more suitable for high fiber concentrations. For example, at higher volume fractions, it is sometimes assumed that the two-point conditionally

probability function obeys the so-called thermodynamic "equilibrium radial distribution function" (ERDF), also known as accurately in the Percus–Yevick approximation (Hansen and McDonald [57]; Torquato and Lado [14]), as follows:

$$g\left(\widehat{r}\right) = H\left(\widehat{r}-1\right)\left[1 + A\left(\widehat{r}\right)\phi\right]; \quad \widehat{r} \equiv r/\left(a_1 + a_2\right), \tag{66}$$

$$\begin{aligned} A\left(\widehat{r}\right) &= \frac{4}{\pi}\left[\pi - 2\sin^{-1}\left(\frac{\widehat{r}}{2}\right) - \widehat{r}\left(1 - \frac{\widehat{r}^2}{4}\right)^{1/2}\right] H\left(2-\widehat{r}\right), \\ H(x) &= \begin{cases} 0, & \text{if } x \le 0, \\ 1, & \text{if } x > 0. \end{cases} \end{aligned} \tag{67}$$

Formulation II: We write

$$\left\langle \bar{\boldsymbol{\varepsilon}}^*_{(1)} \right\rangle^{\mathrm{GII}} = \underset{\sim}{\boldsymbol{\Gamma}}^{\mathrm{GII}}_{(1)} : \boldsymbol{\varepsilon}^{*0}_{(1)}, \tag{68}$$

$$\underset{\sim}{\boldsymbol{\Gamma}}^{\mathrm{GII}}_{(1)} = \gamma^{\mathrm{GII}}_{11}\delta_{ij}\delta_{kl} + \gamma^{\mathrm{GII}}_{21}\left(\delta_{ik}\delta_{jl} + \delta_{il}\delta_{jk}\right), \tag{69}$$

$$\gamma^{\mathrm{GII}}_{11} = \frac{\phi^{(2)}}{4}\mathbf{U}^{\mathrm{GII}}_{21} + \frac{\phi^{(1)}}{4}\mathbf{U}^{\mathrm{GII}}_{11}; \quad \gamma^{\mathrm{GII}}_{21} = \frac{1}{2} + \frac{\phi^{(2)}}{4}\mathbf{V}^{\mathrm{GII}}_{21} + \frac{\phi^{(1)}}{4}\mathbf{V}^{\mathrm{GII}}_{11}, \tag{70}$$

$$\begin{aligned} \mathbf{U}^{\mathrm{GII}}_{21} &= f^{\mathrm{G}}_{11} + \left(\frac{1}{\beta_1\beta_2}\right)\left[24\left(2\lambda^4 + \lambda^2\right)\mathrm{Y}_{32}(g) - 36\left(\lambda^6 + \lambda^4\right)\mathrm{Y}_{52}(g)\right], \\ \mathbf{U}^{\mathrm{GII}}_{11} &= t^{\mathrm{G}}_{11} + \left(\frac{1}{\beta_1^2}\right)\left[72\mathrm{Y}_{31}(g) - 72\mathrm{Y}_{51}(g)\right], \end{aligned} \tag{71}$$

$$\begin{aligned} \mathbf{V}^{\mathrm{GII}}_{21} &= f^{\mathrm{G}}_{21} + \left(\frac{1}{\beta_1\beta_2}\right)\left[-24\left(2\lambda^4 + \lambda^2\right)\mathrm{Y}_{32}(g) + 36\left(\lambda^6 + \lambda^4\right)\mathrm{Y}_{52}(g)\right], \\ \mathbf{V}^{\mathrm{GII}}_{11} &= t^{\mathrm{G}}_{21} + \left(\frac{1}{\beta_1^2}\right)\left[-72\mathrm{Y}_{31}(g) + 72\mathrm{Y}_{51}(g)\right], \end{aligned} \tag{72}$$

$$\begin{aligned} \mathrm{Y}_{32}(g) &= \int_0^{\frac{1}{1+\lambda}} \rho_2^3 g(\rho_2)\mathrm{d}\rho_2; \quad \mathrm{Y}_{52}(g) = \int_0^{\frac{1}{1+\lambda}} \rho_2^5 g(\rho_2)\,\mathrm{d}\rho_2, \\ \mathrm{Y}_{31}(g) &= \int_0^{\frac{1}{2}} \rho_1^3 g(\rho_1)\,\mathrm{d}\rho_1; \quad \mathrm{Y}_{51}(g) = \int_0^{\frac{1}{2}} \rho_1^5 g(\rho_1)\mathrm{d}\rho_1, \end{aligned} \tag{73}$$

Similarly, we have

$$\left\langle \bar{\boldsymbol{\varepsilon}}^*_{(2)} \right\rangle^{\mathrm{GII}} = \underset{\sim}{\boldsymbol{\Gamma}}^{\mathrm{GII}}_{(2)} : \boldsymbol{\varepsilon}^{*0}_{(2)}, \tag{74}$$

$$\underset{\sim}{\boldsymbol{\Gamma}}^{\mathrm{GII}}_{(2)} = \gamma^{\mathrm{GII}}_{12}\delta_{ij}\delta_{kl} + \gamma^{\mathrm{GII}}_{22}\left(\delta_{ik}\delta_{jl} + \delta_{il}\delta_{jk}\right), \tag{75}$$

$$\gamma^{\mathrm{GII}}_{12} = \frac{\phi^{(1)}}{4}\mathbf{U}^{\mathrm{GII}}_{12} + \frac{\phi^{(2)}}{4}\mathbf{U}^{\mathrm{GII}}_{22}; \quad \gamma^{\mathrm{GII}}_{22} = \frac{1}{2} + \frac{\phi^{(1)}}{4}\mathbf{V}^{\mathrm{GII}}_{12} + \frac{\phi^{(2)}}{4}\mathbf{V}^{\mathrm{GII}}_{22}, \tag{76}$$

$$\begin{aligned} \mathbf{U}^{\mathrm{GII}}_{12} &= f^{\mathrm{G}}_{12} + \left(\frac{1}{\beta_1\beta_2}\right)\left[24\left(2\eta^4 + \eta^2\right)\mathrm{P}_{31}(g) - 36\left(\eta^6 + \eta^4\right)\mathrm{P}_{51}(g)\right], \\ \mathbf{U}^{\mathrm{GII}}_{22} &= t^{\mathrm{G}}_{12} + \left(\frac{1}{\beta_2^2}\right)\left[72\mathrm{P}_{32}(g) - 72\mathrm{P}_{52}(g)\right], \end{aligned} \tag{77}$$

$$\begin{aligned}
\mathbf{V}_{12}^{\mathrm{GII}} &= f_{22}^{\mathrm{G}} + \left(\frac{1}{\beta_1\beta_2}\right)\left[-24\left(2\eta^4+\eta^2\right)\mathrm{P}_{31}(g) + 36\left(\eta^6+\eta^4\right)\mathrm{P}_{51}(g)\right],\\
\mathbf{V}_{22}^{\mathrm{GII}} &= t_{22}^{\mathrm{G}} + \left(\frac{1}{\beta_2^2}\right)\left[-72\mathrm{P}_{32}(g) + 72\mathrm{P}_{52}(g)\right],
\end{aligned} \tag{78}$$

$$\begin{aligned}
\mathrm{P}_{31}(g) &= \int_0^{\frac{1}{1+\eta}} \rho_1^3 g(\rho_1)\,\mathrm{d}\rho_1; \quad \mathrm{P}_{51}(g) = \int_0^{\frac{1}{1+\eta}} \rho_1^5 g(\rho_1)\,\mathrm{d}\rho_1,\\
\mathrm{P}_{32}(g) &= \int_0^{\frac{1}{2}} \rho_2^3 g(\rho_2)\,\mathrm{d}\rho_2; \quad \mathrm{P}_{52}(g) = \int_0^{\frac{1}{2}} \rho_2^5 g(\rho_2)\,\mathrm{d}\rho_2.
\end{aligned} \tag{79}$$

Formulation I: We write

$$\left\langle \bar{\boldsymbol{\varepsilon}}_{(1)}^{*} \right\rangle^{\mathrm{GI}} = \underset{\sim}{\boldsymbol{\Gamma}}_{(1)}^{\mathrm{GI}} : \boldsymbol{\varepsilon}_{(1)}^{*0}, \tag{80}$$

$$\underset{\sim}{\boldsymbol{\Gamma}}_{(1)}^{\mathrm{GI}} = \gamma_{11}^{\mathrm{GI}}\delta_{ij}\delta_{kl} + \gamma_{21}^{\mathrm{GI}}\left(\delta_{ik}\delta_{jl}+\delta_{il}\delta_{jk}\right), \tag{81}$$

$$\gamma_{11}^{\mathrm{GI}} = \frac{\phi^{(2)}}{4}\mathbf{U}_{21}^{\mathrm{GI}} + \frac{\phi^{(1)}}{4}\mathbf{U}_{11}^{\mathrm{GI}}; \quad \gamma_{21}^{\mathrm{GI}} = \frac{1}{2} + \frac{\phi^{(2)}}{4}\mathbf{V}_{21}^{\mathrm{GI}} + \frac{\phi^{(1)}}{4}\mathbf{V}_{11}^{\mathrm{GI}}, \tag{82}$$

$$\mathbf{U}_{21}^{\mathrm{GI}} = f_{11}^{\mathrm{G}}; \quad \mathbf{U}_{11}^{\mathrm{GI}} = t_{11}^{\mathrm{G}}; \quad \mathbf{V}_{21}^{\mathrm{GI}} = f_{21}^{\mathrm{G}}; \quad \mathbf{V}_{11}^{\mathrm{GI}} = t_{21}^{\mathrm{G}}, \tag{83}$$

$$\begin{aligned}
f_{11}^{\mathrm{G}} &= \frac{\omega_{11}}{\beta_1\beta_2}\mathrm{Y}_{12}(g)\,4\lambda^2; \quad t_{11}^{\mathrm{G}} = \frac{4S_{11}}{\beta_1^2}\mathrm{Y}_{11}(g),\\
f_{21}^{\mathrm{G}} &= \frac{\omega_{12}}{\beta_1\beta_2}\mathrm{Y}_{12}(g)\,4\lambda^2; \quad t_{21}^{\mathrm{G}} = \frac{4S_{12}}{\beta_1^2}\mathrm{Y}_{11}(g),
\end{aligned} \tag{84}$$

$$\begin{aligned}
\omega_{11} &= \frac{-2\left\{\alpha_1\left[2\alpha_2+(3-2\nu_0)\beta_2\right]+\beta_1\left[4\nu_0\alpha_2+(2\nu_0+1)\beta_2\right]\right\}}{(\alpha_1+\beta_1)(\alpha_2+\beta_2)},\\
\omega_{12} &= \frac{2\left[2\alpha_2+(3-2\nu_0)\beta_2\right]}{\alpha_2+\beta_2}; \quad S_{11} = 2\left[-2+\frac{(1-2\nu_0)\beta_1}{\alpha_1+\beta_1}\right]; \quad S_{12} = 2\left[2+\frac{(1-2\nu_0)\beta_1}{\alpha_1+\beta_1}\right],
\end{aligned} \tag{85}$$

$$\mathrm{Y}_{11}(g) = \int_0^{\frac{1}{2}} \rho_1 g(\rho_1)\,\mathrm{d}\rho_1; \quad \mathrm{Y}_{12}(g) = \int_0^{\frac{1}{1+\lambda}} \rho_2 g(\rho_2)\,\mathrm{d}\rho_2. \tag{86}$$

Similarly, we obtain

$$\left\langle \bar{\boldsymbol{\varepsilon}}_{(2)}^{*} \right\rangle^{\mathrm{GI}} = \underset{\sim}{\boldsymbol{\Gamma}}_{(2)}^{\mathrm{GI}} : \boldsymbol{\varepsilon}_{(2)}^{*0}, \tag{87}$$

$$\underset{\sim}{\boldsymbol{\Gamma}}_{(2)}^{\mathrm{GI}} = \gamma_{12}^{\mathrm{GI}}\delta_{ij}\delta_{kl} + \gamma_{22}^{\mathrm{GI}}\left(\delta_{ik}\delta_{jl}+\delta_{il}\delta_{jk}\right), \tag{88}$$

$$\gamma_{12}^{\mathrm{GI}} = \frac{\phi^{(1)}}{4}\mathbf{U}_{12}^{\mathrm{GI}} + \frac{\phi^{(2)}}{4}\mathbf{U}_{22}^{\mathrm{GI}}; \quad \gamma_{22}^{\mathrm{GI}} = \frac{1}{2} + \frac{\phi^{(1)}}{4}\mathbf{V}_{12}^{\mathrm{GI}} + \frac{\phi^{(2)}}{4}\mathbf{V}_{22}^{\mathrm{GI}}, \tag{89}$$

$$\mathbf{U}_{12}^{\mathrm{GI}} = f_{12}^{\mathrm{G}}; \quad \mathbf{U}_{22}^{\mathrm{GI}} = t_{12}^{\mathrm{G}}; \quad \mathbf{V}_{12}^{\mathrm{GI}} = f_{22}^{\mathrm{G}}; \quad \mathbf{V}_{22}^{\mathrm{GI}} = t_{22}^{\mathrm{G}}, \tag{90}$$

$$\begin{aligned}
f_{12}^{\mathrm{G}} &= \frac{e_{11}}{\beta_1\beta_2}\mathrm{P}_{11}(g)\,4\eta^2; \quad t_{12}^{\mathrm{G}} = \frac{4g_{11}}{\beta_2^2}\mathrm{P}_{12}(g),\\
f_{22}^{\mathrm{G}} &= \frac{e_{12}}{\beta_1\beta_2}\mathrm{P}_{11}(g)\,4\eta^2; \quad t_{22}^{\mathrm{G}} = \frac{4g_{12}}{\beta_2^2}\mathrm{P}_{12}(g),
\end{aligned} \tag{91}$$

$$
\begin{aligned}
e_{11} &= \frac{-2\left\{\alpha_2\left[2\alpha_1+(3-2\nu_0)\,\beta_1\right]+\beta_2\left[4\nu_0\alpha_1+(2\nu_0+1)\,\beta_1\right]\right\}}{(\alpha_1+\beta_1)\,(\alpha_2+\beta_2)},\\
e_{12} &= \frac{2\left[2\alpha_1+(3-2\nu_0)\,\beta_1\right]}{\alpha_1+\beta_1};\quad g_{11}=2\left[-2+\frac{(1-2\nu_0)\,\beta_2}{\alpha_2+\beta_2}\right],\\
g_{12} &= 2\left[2+\frac{(1-2\nu_0)\,\beta_2}{\alpha_2+\beta_2}\right],
\end{aligned}
\tag{92}
$$

$$
\mathrm{P}_{11}(g)=\int_0^{\frac{1}{1+\eta}}\rho_1 g(\rho_1)\,\mathrm{d}\rho_1;\quad \mathrm{P}_{12}(g)=\int_0^{\frac{1}{2}}\rho_2 g(\rho_2)\,\mathrm{d}\rho_2. \tag{93}
$$

4 Effective transverse elastic moduli of two-phase composites containing unidirectionally aligned circular fibers

In this section, we derive effective transverse elastic moduli of composites containing many randomly dispersed unidirectionally aligned fibers with same properties and sizes in two-phase composites. We shall utilize the probabilistic ensemble-area averaged pairwise local interaction solution for $\left\langle \bar{\boldsymbol{\varepsilon}}^*_{(i)}\right\rangle$ and other ensemble-area averaged field equations. In what follows, angular brackets for the ensemble-area operators will be dropped for compactness. According to Ju and Chen [25] and Zhao et al. [58], the following relations governing the ensemble-area averaged stress $\bar{\boldsymbol{\sigma}}$, the averaged strain $\bar{\boldsymbol{\varepsilon}}$, the uniform remote strain $\boldsymbol{\varepsilon}^0$ and the averaged eigenstrain $\bar{\boldsymbol{\varepsilon}}^*_{(i)}$take the form:

$$
\bar{\boldsymbol{\sigma}}=\mathbf{C}_0:\left(\bar{\boldsymbol{\varepsilon}}-\sum_{i=1}^{2}\phi^{(i)}\bar{\boldsymbol{\varepsilon}}^*_{(i)}\right), \tag{94}
$$

$$
\bar{\boldsymbol{\varepsilon}}=\boldsymbol{\varepsilon}^0+\sum_{i=1}^{2}\phi^{(i)}\mathbf{S}:\bar{\boldsymbol{\varepsilon}}^*_{(i)}, \tag{95}
$$

$$
\begin{aligned}
\bar{\boldsymbol{\sigma}}=\bar{\mathbf{C}}:\bar{\boldsymbol{\varepsilon}} &= \left[\mathbf{C}_0\bullet\left(\mathbf{I}-\phi^{(1)}\underset{\sim}{\boldsymbol{\Gamma}}^{\mathbf{II}}_{(1)}\underset{\sim}{\mathbf{U}}^{\mathbf{II}^{-1}}_{(1)}-\phi^{(2)}\underset{\sim}{\boldsymbol{\Gamma}}^{\mathbf{II}}_{(2)}\underset{\sim}{\mathbf{U}}^{\mathbf{II}^{-1}}_{(2)}\right)\right]:\bar{\boldsymbol{\varepsilon}}\\
&= \left[\bar{\lambda}\delta_{ij}\delta_{kl}+\bar{\mu}_T\left(\delta_{ik}\delta_{jl}+\delta_{il}\delta_{jk}\right)\right]:\bar{\varepsilon}_{kl};\qquad i,j,k,l=1,2,
\end{aligned}
\tag{96}
$$

where the following relations are employed to derive $\bar{\mathbf{C}}$:

$$
\bar{\boldsymbol{\varepsilon}}=\underset{\sim}{\mathbf{U}}^{\mathbf{II}}_{(1)}:\boldsymbol{\varepsilon}^{*0}_{(1)}=\left[-\mathbf{A}_1-\mathbf{S}+\phi^{(1)}\mathbf{S}\bullet\underset{\sim}{\boldsymbol{\Gamma}}^{\mathbf{II}}_{(1)}+\phi^{(2)}\mathbf{S}\bullet\underset{\sim}{\boldsymbol{\Gamma}}^{\mathbf{II}}_{(2)}\left(\mathbf{A}_2+\mathbf{S}\right)^{-1}\left(\mathbf{A}_1+\mathbf{S}\right)\right]:\boldsymbol{\varepsilon}^{*0}_{(1)}, \tag{97}
$$

$$
\bar{\boldsymbol{\varepsilon}}=\underset{\sim}{\mathbf{U}}^{\mathbf{II}}_{(2)}:\boldsymbol{\varepsilon}^{*0}_{(2)}=\left[-\mathbf{A}_2-\mathbf{S}+\phi^{(1)}\mathbf{S}\bullet\underset{\sim}{\boldsymbol{\Gamma}}^{\mathbf{II}}_{(1)}\left(\mathbf{A}_2+\mathbf{S}\right)\left(\mathbf{A}_1+\mathbf{S}\right)^{-1}+\phi^{(2)}\mathbf{S}\bullet\underset{\sim}{\boldsymbol{\Gamma}}^{\mathbf{II}}_{(2)}\right]:\boldsymbol{\varepsilon}^{*0}_{(2)}. \tag{98}
$$

Since all the fourth-rank tensors on the right-hand side of Eq. (96) are isotropic in two dimensions, the effective stiffness tensor $\bar{\mathbf{C}}$ for these *three-phase* composites is also isotropic in 2-D (or, equivalently transversely isotropic in three dimensions). For the *two-phase* composites, simply let the two inhomogeneity phases have the *same* elastic properties and sizes within the proposed framework for three-phase composites. It is noted that based on Eqs. (54)–(65) and Eqs. (80)–(93) in our Formulation I for the two-phase composites, we can prove that $\gamma_1=\gamma^{\mathbf{I}}_{11}=\gamma^{\mathbf{I}}_{12}$ and $\gamma_2=\gamma^{\mathbf{I}}_{21}=\gamma^{\mathbf{I}}_{22}$. Therefore, we can recover Eqs. (38)–(39) and (48)–(49) in Ju and Zhang [27].

4.1 Uniform radial distribution function (URDF)

Accordingly, the effective *plane-strain* bulk modulus $\bar{k}_T$ and the shear modulus $\bar{\mu}_T$ of two-phase composites can be explicitly evaluated as:

$$\bar{k}_T^{\mathrm{UII}} = k_0 \left\{ 1 + \frac{8\phi\,(1-\nu_0)\left[\left(\gamma_1^{\mathrm{UII}} + \gamma_2^{\mathrm{UII}}\right)\right]}{(\alpha+\beta) - \left[4\phi\left(\gamma_1^{\mathrm{UII}} + \gamma_2^{\mathrm{UII}}\right)\right]} \right\}; \; \bar{\mu}_T^{\mathrm{UII}} = \mu_0 \left\{ 1 + \frac{8\phi\,(1-\nu_0)\,\gamma_2^{\mathrm{UII}}}{\beta - 2\,(3-4\nu_0)\,\phi\gamma_2^{\mathrm{UII}}} \right\}, \tag{99}$$

$$\alpha = 4\,(1-\nu_0)\left[\frac{k_0}{k_1-k_0} - \frac{\mu_0}{\mu_1-\mu_0}\right] + (4\nu_0 - 1)\,; \; \beta = 4\,(1-\nu_0)\,\frac{\mu_0}{\mu_1-\mu_0} + (3-4\nu_0)\,. \tag{100}$$

It is noted that the definition of the effective plane-strain bulk modulus is $\bar{k}_T \equiv \bar{\lambda} + \bar{\mu}_T$, where $\bar{\lambda}$ and $\bar{\mu}_T$ are the effective Lamé constants. The proposed micromechanical plane-strain framework cannot predict the effective axial (out-of-plane) Young's modulus $\bar{E}_A$ and effective Poisson's ratio $\bar{\nu}_A$. On the other hand, bounds on effective axial $\bar{E}_A$ and $\bar{\nu}_A$ are available from Hashin [10]:

$$\bar{E}_A = E_0\phi^{(0)} + E_1\phi + \frac{4\phi\phi^{(0)}\,(\nu_1-\nu_0)^2}{\frac{\phi}{k_0} + \frac{\phi^{(0)}}{k_1} + \frac{1}{\mu_0}}, \tag{101}$$

$$\bar{\nu}_A = \nu_0\phi^{(0)} + \nu_1\phi + \frac{\phi\phi^{(0)}\,(\nu_1-\nu_0)\,(1/k_0 - 1/k_1)}{\frac{\phi}{k_0} + \frac{\phi^{(0)}}{k_1} + \frac{1}{\mu_0}}, \tag{102}$$

where $\phi^{(0)} \equiv 1-\phi$. According to the calculations of Kondo and Saito [59] and Ju and Zhang [27], Eqs. (101) and (102) render highly accurate predictions because the lower and upper bound of Hashin [10] are extremely close to each other. Even a simple mixture rule (the first two terms on the right-hand side of Eqs. (101) and (102)) provides fairly good estimates for effective axial $\bar{E}_A$ and $\bar{\nu}_A$. Therefore, the out-of-plane fiber interaction effects are insignificant as far as $\bar{E}_A$ and $\bar{\nu}_A$ are concerned. Consequently, the effective *transverse* Young's modulus $\bar{E}_T$ and Poisson's ratio $\bar{\nu}_T$ can be predicted by combining our Eqs. (99)–(100) for $\bar{k}_T$ and $\bar{\mu}_T$ and Eqs. (101)–(102) for $\bar{E}_A$ and $\bar{\nu}_A$:

$$\bar{E}_T^{\mathrm{UII}} = \frac{4\bar{k}_T^{\mathrm{UII}}\bar{\mu}_T^{\mathrm{UII}}}{\bar{k}_T^{\mathrm{UII}} + \varphi^{\mathrm{UII}}\bar{\mu}_T^{\mathrm{UII}}}; \quad \bar{\nu}_T^{\mathrm{UII}} = \frac{\bar{k}_T^{\mathrm{UII}} - \varphi\bar{\mu}_T^{\mathrm{UII}}}{\bar{k}_T^{\mathrm{UII}} + \varphi^{\mathrm{UII}}\bar{\mu}_T^{\mathrm{UII}}}; \quad \varphi^{\mathrm{UII}} = 1 + \frac{4\bar{\nu}_A^2\bar{k}_T^{\mathrm{UII}}}{\bar{E}_A}. \tag{103}$$

The above expressions were given by Hashin and Rosen [5]; see Eqs. (17)–(18) therein. We can simply replace superscript "II" by "I" in Formulation II to obtain Formulation I. Our Formulation I equations are entirely identical to Eqs. (48)–(49) and Eqs. (58)–(59) in Ju and Zhang [27] with $\mathrm{Y}(g) = 1/8$ therein.

4.2 General radial distribution function (GRDF)

In this event, we arrive at

$$\bar{k}_T^{\mathrm{GII}} = k_0 \left\{ 1 + \frac{8\phi\,(1-\nu_0)\left[\left(\gamma_1^{\mathrm{GII}} + \gamma_2^{\mathrm{GII}}\right)\right]}{(\alpha+\beta) - \left[4\phi\left(\gamma_1^{\mathrm{GII}} + \gamma_2^{\mathrm{GII}}\right)\right]} \right\}, \tag{104}$$

$$\bar{\mu}_T^{\mathrm{GII}} = \mu_0 \left\{ 1 + \frac{8\phi\,(1-\nu_0)\,\gamma_2^{\mathrm{GII}}}{\beta - 2\,(3-4\nu_0)\,\phi\gamma_2^{\mathrm{GII}}} \right\}, \tag{105}$$

$$\bar{E}_T^{\mathrm{GII}} = \frac{4\bar{k}_T^{\mathrm{GII}}\bar{\mu}_T^{\mathrm{GII}}}{\bar{k}_T^{\mathrm{GII}} + \varphi^{\mathrm{GII}}\bar{\mu}_T^{\mathrm{GII}}}; \quad \bar{\nu}_T^{\mathrm{GII}} = \frac{\bar{k}_T^{\mathrm{GII}} - \varphi\bar{\mu}_T^{\mathrm{GII}}}{\bar{k}_T^{\mathrm{GII}} + \varphi^{\mathrm{GII}}\bar{\mu}_T^{\mathrm{GII}}}; \quad \varphi^{\mathrm{GII}} = 1 + \frac{4\bar{\nu}_A^2\bar{k}_T^{\mathrm{GII}}}{\bar{E}_A}, \tag{106}$$

$$\begin{aligned} \mathrm{Y}_{32}(g) = \mathrm{Y}_{31}(g) = \mathrm{P}_{31}(g) = \mathrm{P}_{32}(g) = \frac{1}{64} + 0.0158\phi, \\ \mathrm{Y}_{52}(g) = \mathrm{Y}_{51}(g) = \mathrm{P}_{51}(g) = \mathrm{P}_{52}(g) = \frac{1}{384} + 0.00307\phi. \end{aligned} \tag{107}$$

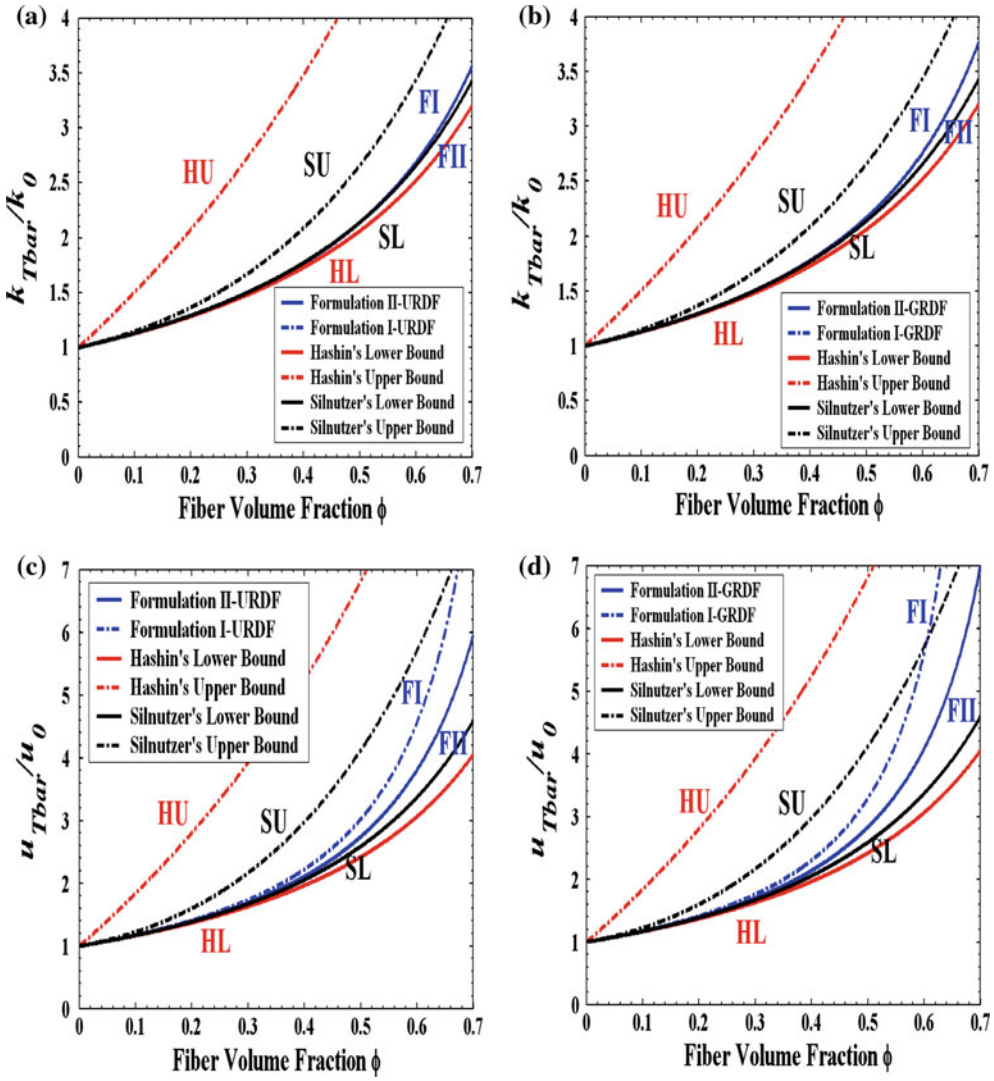

Fig. 3 An elastic matrix with elastic cylindrical fibers: the effective plane-strain bulk modulus ($\bar{k}_T/k_0$) versus the fiber volume fraction ϕ: **a** URDF, **b** GRDF/ERDF; the effective transverse shear modulus ($\bar{\mu}_T/\mu_0$) versus the fiber volume fraction ϕ: **c** URDF, **d** GRDF/ERDF

To obtain Formulation I, we can simply replace the superscript "II" by "I" in Formulation II. Again, our Formulation I equations are entirely identical to Eqs. (48)–(49) and Eqs. (58)–(59) in Ju and Zhang [27] with $\mathrm{Y}(g) = \frac{1}{8} + 0.0865\phi$ therein. In addition, we have

$$\mathrm{Y}_{12}(g) = \mathrm{Y}_{11}(g) = \mathrm{P}_{11}(g) = \mathrm{P}_{12}(g) = \frac{1}{8} + 0.0865\phi \equiv \mathrm{Y}(g). \tag{108}$$

5 Some comparisons and numerical simulations

In the illustrations, the following notations will be employed: "HU", "HL", "SU", "SL", "FI", "FII", "FIU", "FIG", "FIIU", and "FIIG" stand for Hashin's upper bound, Hashin's lower bound, Silnutzer's upper bound, Silnutzer's lower bound, Formulation I, Formulation II, Formulation I based on the URDF, Formulation I based on the GRDF/ERDF, Formulation II based on the URDF, and Formulation II based on the GRDF/ERDF, respectively.

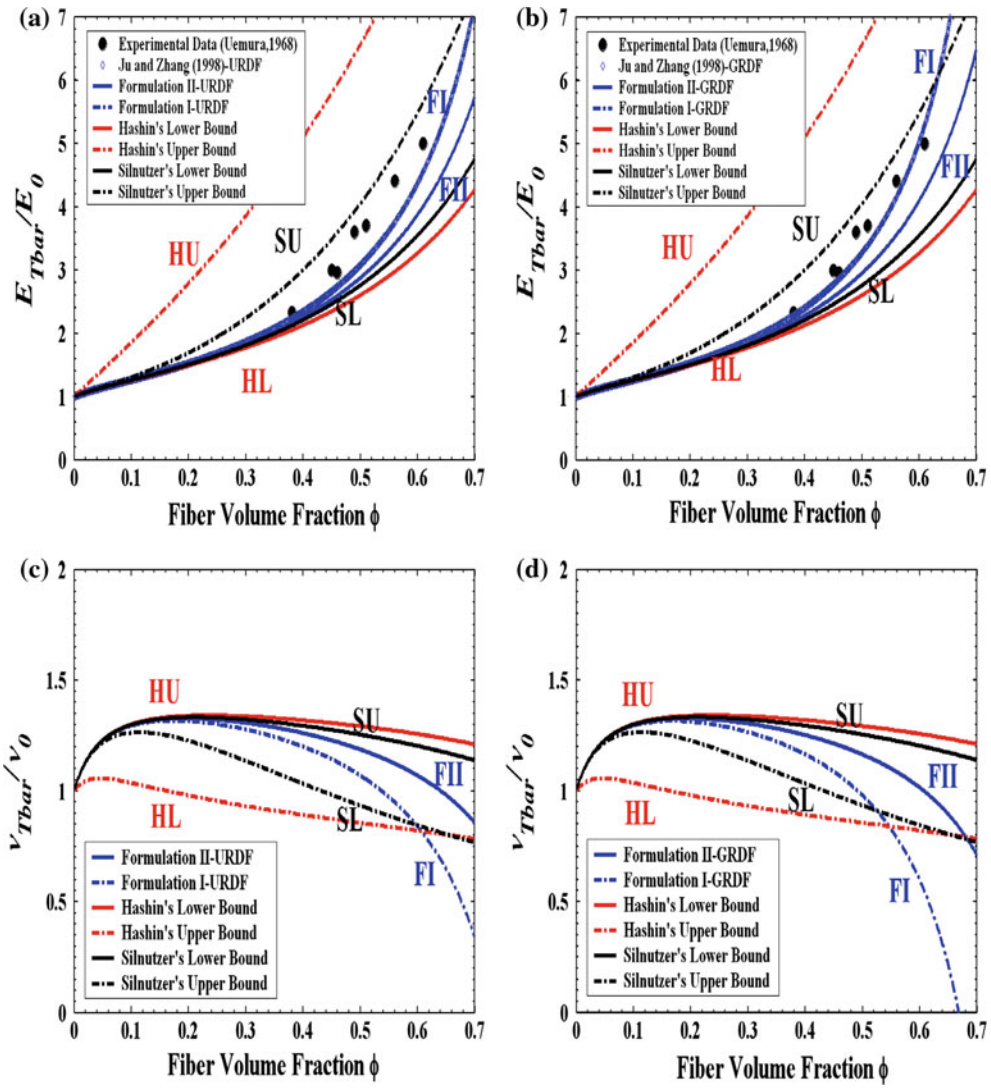

Fig. 4 An elastic matrix with elastic cylindrical fibers: the effective transverse Young's modulus ($\bar{E}_T/E_0$) versus the fiber volume fraction ϕ: **a** URDF, **b** GRDF/ERDF; the effective transverse Poisson's ratio ($\bar{\nu}_T/\nu_0$) versus the fiber volume fraction ϕ: **c** URDF, **d** GRDF/ERDF

5.1 Elastic matrix with elastic cylindrical fibers

Following Kondo and Saito [59], we consider the following constituent elastic phase properties for the glass fiber-reinforced epoxy matrix composites: $E_1 = 114.35$ GPa, $\nu_1 = 0.22$ (glass fiber) and $E_0 = 5.39$ GPa, $\nu_0 = 0.35$ (epoxy resin). The effective plane-strain bulk modulus ($\bar{k}_T/k_0$) versus the fiber volume fraction based on the URDF and the GRDF/ERDF are rendered in Fig. 3a, b, respectively. The prediction based on FI is very close to that based on FII. The prediction based on the GRDF/ERDF provides a higher value in Fig. 3b than that based on the URDF in Fig. 3a. The effective transverse shear modulus ($\bar{\mu}_T/\mu_0$) versus the fiber volume fractions based on the URDF and the GRDF/ERDF are displayed in Fig. 3c, d, respectively. The prediction based on FI is higher than that based on FII. Thus, the FI forms the higher-order upper bound and FII forms the higher-order lower bound. It is noted that the FI based on the GRDF/ERDF violates the SU at a fiber volume fraction of 60 %. In addition, the prediction based on the GRDF/ERDF provides a higher value in Fig. 3d than that based on the URDF in Fig. 3c. The effective transverse Young's modulus ($\bar{E}_T/E_0$) versus the fiber volume fraction based on the URDF and the GRDF/ERDF is exhibited in Fig. 4a, b, respectively. The prediction based on FI (identical to Ju and Zhang [27]) is higher than that based on FII. Therefore, the FI forms the higher-order upper bound and FII forms the higher-order lower bound. It is observed that the FI

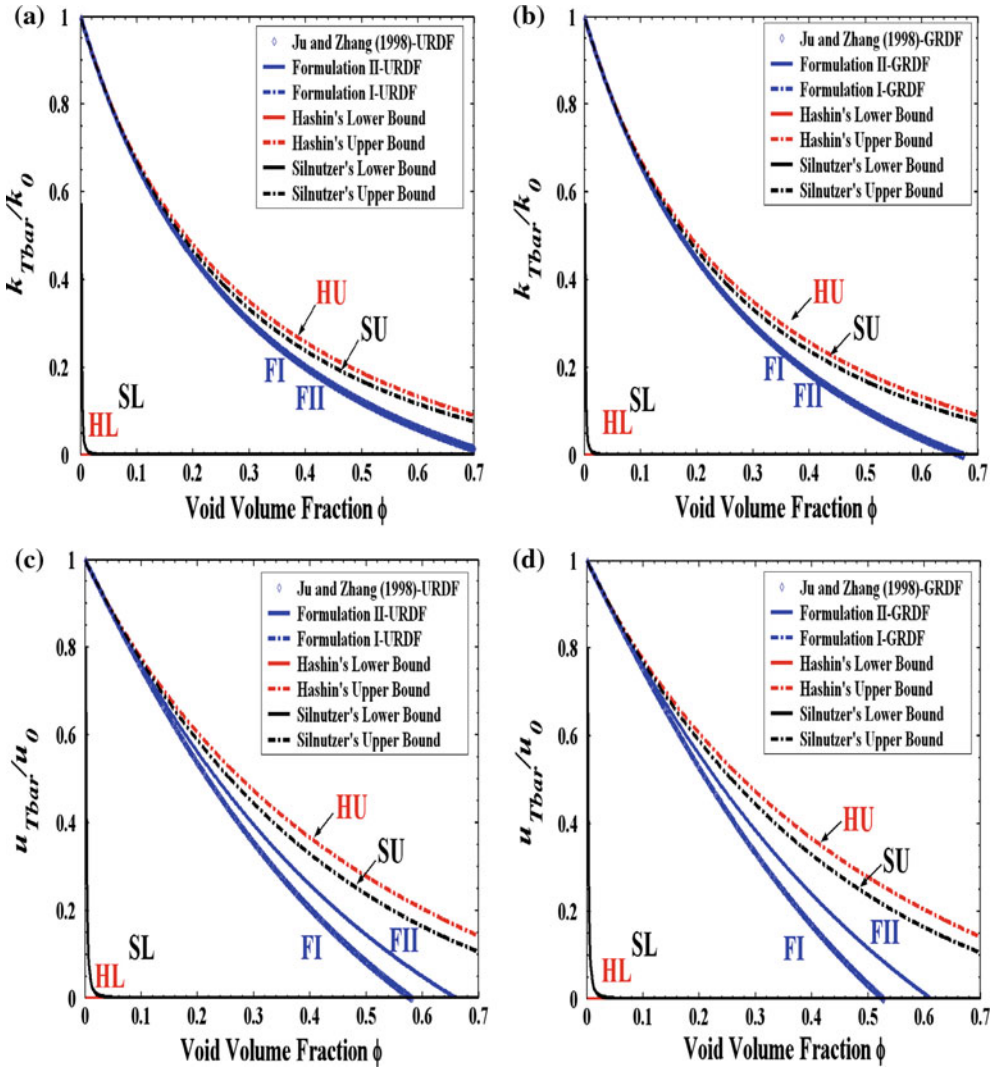

Fig. 5 An elastic matrix with cylindrical voids: the effective plane-strain bulk modulus ($\bar{k}_T/k_0$) versus the void volume fraction ϕ: **a** URDF, **b** GRDF/ERDF; the effective transverse shear modulus ($\bar{\mu}_T/\mu_0$) versus the void volume fraction ϕ: **c** URDF, **d** GRDF/ERDF

based on the GRDF/ERDF violates the SU at a fiber volume fraction of 64 %. In addition, the prediction based on the GRDF/ERDF provides a higher value in Fig. 4b than that based on the URDF in Fig. 4a. Furthermore, the prediction based on the GRDF/ERDF matches well with the experimental data by Uemura et al. [60] at higher fiber volume fractions (above fiber volume fractions of 40 %). The effective transverse Poisson's ratio ($\bar{\nu}_T/\nu_0$) versus the fiber volume fraction based on the URDF and the GRDF/ERDF is rendered in Fig. 4c, d, respectively. The prediction based on FII is higher than that based on FI in this case. Therefore, the FII forms the higher-order upper bound and FI forms the higher-order lower bound. We note that the FI based on the URDF and the GRDF/ERDF violates the SL at fiber volume fractions of 60 and 54 %, respectively.

5.2 Elastic matrix with cylindrical voids

We now consider the following constituent elastic phase properties for the cylindrical voids in the epoxy matrix composites: $k_1 \to 0$ GPa, $\mu_1 \to 0$ (voids) and $E_0 = 5.39$ GPa, $\nu_0 = 0.35$ (epoxy resin). The effective plane-strain bulk modulus ($\bar{k}_T/k_0$) versus the void volume fraction based on the URDF and the GRDF/ERDF are displayed in Fig. 5a, b, respectively. The prediction based on FI (identical to Ju and Zhang [27]) is very close to that based on FII. As expected, the effective plane-strain bulk modulus decreases as the void volume

fraction increases. The prediction based on the GRDF/ERDF decreases faster in Fig. 5b than that based on the URDF in Fig. 5a. The effective transverse shear modulus ($\bar{\mu}_T/\mu_0$) versus the void volume fraction based on the URDF and the GRDF/ERDF are exhibited in Fig. 5c, d, respectively. The prediction based on FII is higher than that based on FI (identical to Ju and Zhang [27]). Thus, the FII forms the higher-order upper bound and FI forms the higher-order lower bound. Bounds are reversed when compared with those in Fig. 3c, d since the inclusions now are replaced by voids. As expected, the effective transverse shear modulus decreases as the void volume fraction increases. The prediction based on the GRDF/ERDF decreases faster in Fig. 5d than that based on the URDF in Fig. 5c.

5.3 Incompressible matrix with cylindrical rigid fibers

As indicated by Christensen [61], the manufacturing operations for fiber composite materials often involve the flow behavior of the composite system as viscous fluid suspensions. The matrix phase is usually treated as incompressible in its fluid sate, and the aligned fibers are treated as rigid (in comparison with the matrix). Therefore, the (rheological) effective transverse shear viscosity $\bar{\eta}_T$ of these composite melts can be represented by the proposed Eqs. (100) and (105), where the solutions for formulation I can be simply obtained by replacing the superscript "II" by "I".

(1) **Formulation II** with the URDF (featuring the singularity point at $\phi = 0.722$):

$$\bar{\eta}_T^{\mathrm{UII}} = \mu_0 \left(-1 - \frac{64}{\phi\,(17\phi + 32) - 32} \right). \tag{109}$$

(2) **Formulation II** with the GRDF/ERDF (featuring the singularity point at $\phi = 0.68$):

$$\bar{\eta}_T^{\mathrm{GII}} = \frac{\mu_0 \left\{ [(-0.2337\phi - 0.5313)\,\phi - 1]\,\phi - 1 \right\}}{[(0.2337\phi + 0.5313)\,\phi + 1]\,\phi - 1}. \tag{110}$$

(3) **Formulation I:**

$$\bar{\eta}_T^{\mathrm{I}} = \mu_0 \left(1 + 2\phi \frac{1 + 8\mathrm{Y}(g)\,\phi}{1 - \phi - 8\mathrm{Y}(g)\,\phi^2} \right). \tag{111}$$

We can prove that, by setting $1 - \phi - 8\mathrm{Y}(g)\,\phi^2 = 0$, for the special cases of the uniform radial distribution function (URDF: $\mathrm{Y}(g) = \frac{1}{8}$) and the general/equilibrium radial distribution function (GRDF/ERDF: $\mathrm{Y}(g) = \frac{1}{8} + 0.0865\phi$), the singularity points in Eq. (111) occur at $\phi = 0.618$ and $\phi = 0.562$, respectively. We note that Eq. (111) is identical to Eq. (63) in Ju and Zhang [27]. It is observed that our FII enhances the singularity points from $\phi = 0.618$ to $\phi = 0.722$ and from $\phi = 0.562$ to $\phi = 0.680$ for the URDF and the GRDF/ERDF, respectively. We now consider the following constituent elastic phase properties for the cylindrical rigid fibers in the incompressible epoxy matrix composites: $k_1 \to \infty\,\mathrm{GPa}$, $\mu_1 \to \infty$ (rigid fibers) and $E_0 = 5.39\,\mathrm{GPa}$, $\nu_0 = 0.5$ (incompressible epoxy resin). Figure 6 compares the theoretical predictions from Hashin [6,10] lower bound, Silnutzer's [11] three-point lower bound (with the equilibrium RDF), and the proposed FI and FII (with the URDF and the GRDF/ERDF). We observe that significant differences exist between our predictions and the other two bounds for ϕ greater than 30 %. No HU and SU are available in this case since those bounds will approach infinity.

5.4 Incompressible matrix with cylindrical voids

In this case, we arrive at the following:

(1) **Formulation II** with the URDF:

$$\bar{k}_T^{\mathrm{UII}} = \mu_0 \left[\frac{2}{2\phi + \phi^2} - 1 \right]; \quad \bar{\mu}_T^{\mathrm{UII}} = \mu_0 \left[\frac{64}{32 + 32\phi + 25\phi^2} - 1 \right]. \tag{112}$$

(2) **Formulation II** with the GRDF/ERDF:

There is no closed-form solution for $\bar{k}_T$ available based on our formulation since $\phi = \phi^{(1)} + \phi^{(2)}$ cannot be obtained. However, numerical solutions can be obtained if numerical values of $\phi^{(1)}$ and $\phi^{(2)}$ are specified.

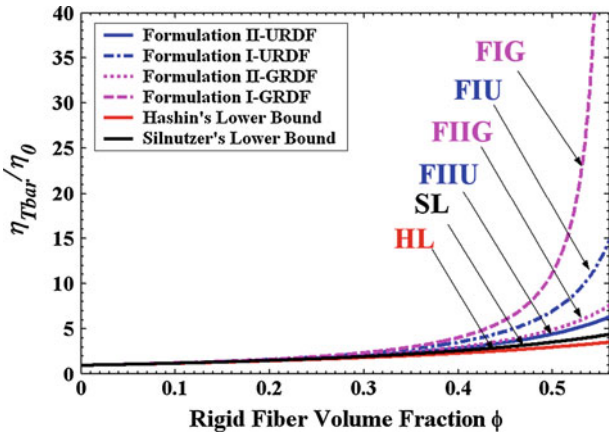

Fig. 6 An incompressible matrix with cylindrical rigid fibers: the effective relative transverse shear viscosity ($\bar{\eta}_T/\eta_0$) versus the rigid fiber volume fraction ϕ

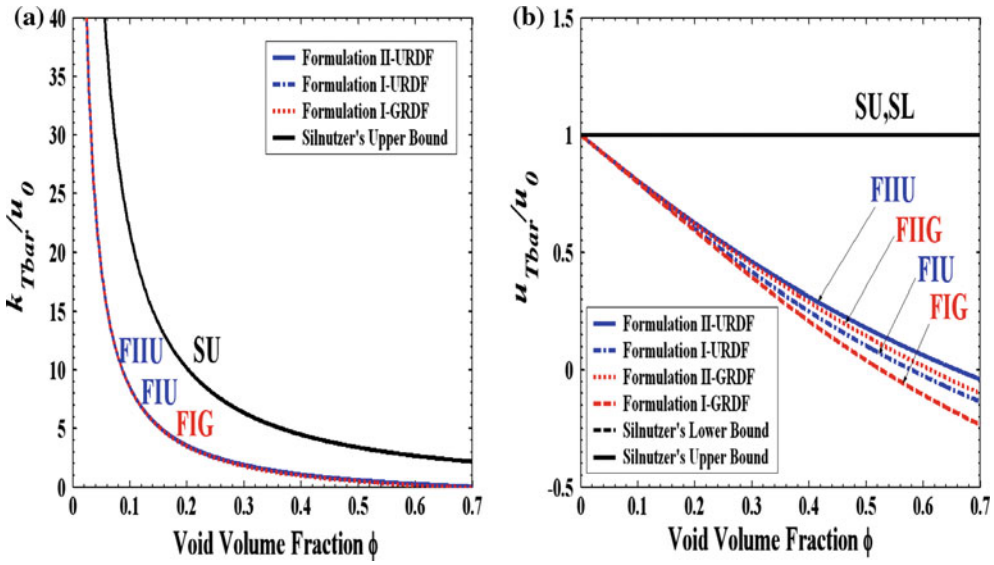

Fig. 7 The incompressible matrix with cylindrical voids: **a** the effective plane-strain bulk modulus ($\bar{k}_T/\mu_0$) versus the void volume fraction ϕ; **b** the effective transverse shear modulus ($\bar{\mu}_T/\mu_0$) versus the void volume fraction ϕ

(3) **Formulation I** with the URDF ($\mathrm{Y}(g) = \frac{1}{8}$):

$$\bar{k}_T^{\mathrm{UI}} = \mu_0 \left[\frac{1}{4\phi^2 \mathrm{Y}(g) + \phi} - 1 \right]; \quad \bar{\mu}_T^{\mathrm{UI}} = \mu_0 \left[1 - \frac{2\phi\,(1 + 10\mathrm{Y}(g)\,\phi)}{1 + \phi + 10\mathrm{Y}(g)\,\phi^2} \right]. \tag{113}$$

(4) **Formulation I** with the GRDF/ERDF ($\mathrm{Y}(g) = \frac{1}{8} + 0.0865\phi$):

$$\bar{k}_T^{\mathrm{GI}} = \mu_0 \left[\frac{1}{4\phi^2 \mathrm{Y}(g) + \phi} - 1 \right]; \quad \bar{\mu}_T^{\mathrm{GI}} = \mu_0 \left[1 - \frac{2\phi\,(1 + 10\mathrm{Y}(g)\,\phi)}{1 + \phi + 10\mathrm{Y}(g)\,\phi^2} \right]. \tag{114}$$

We now consider the following constituent elastic phase properties for the cylindrical voids in the incompressible epoxy matrix composites: $k_1 \to 0\,\mathrm{GPa}$, $\mu_1 \to 0$ (voids) and $E_0 = 5.39\,\mathrm{GPa}$, $\nu_0 = 0.5$ (incompressible epoxy resin). The effective plane-strain bulk modulus ($\bar{k}_T/k_0$) versus the void volume fraction are exhibited in Fig. 7a. The prediction based on FI is very close to that based on FII. No closed-form solution for FIIG is available. As expected, the effective plane-strain bulk modulus decreases as the void volume fraction increases. Both the HU and HL approach infinity in this case. It is also noted that SL does not work well in this case, either. However, our proposed formulations can capture the trend very well. The effective transverse shear

modulus ($\bar{\mu}_T/\mu_0$) versus the void volume fraction are rendered in Fig. 7b. Moreover, the effective transverse shear modulus decreases as the void volume fraction increases. The SU and SL are equal to 1 in this case. Both the HU and HL approach infinity. Nevertheless, our proposed formulations still capture the trend quite well.

6 Conclusions

Based on the governing micromechanical field equations and the approximate (higher-order) pairwise fiber interaction solutions, new higher-order micromechanical formulations have been presented in this work to predict effective transverse elastic moduli of two-phase fiber-reinforced composites containing randomly located and interacting aligned circular fibers with same elastic properties and sizes. The effects of random distribution of circular fibers are accounted for through the probabilistic ensemble averaging process. The ensemble-area averaged eigenstrains in fibers are approximately yet accurately evaluated through the pairwise fiber interactions. Hence, a compact analytical formula is derived. As a result, two non-equivalent formulations of effective transverse elastic moduli have been derived, leading to the new higher-order bounds. The present paper represents a significant improvement over the previous work of Ju and Zhang [27] (and other researchers) which is based on the identical circular fibers in the matrix. Moreover, the present higher-order predictions (in ρ) are compared with those of Ju and Zhang [27], Hashin's second-order bounds [6,10], Silnutzer's third-order bounds [11], and selected experimental data. These comparisons and simulations encompass wide ranges of fiber-reinforced elastic composites including randomly located circular elastic fibers, rigid fibers, and voids. No Monte Carlo simulations or finite element calculations are needed here.

Experimental validations are key parameters in the calibration of proposed models. Further experimental validations and comparisons will be performed once the associated experiment data become available. In the forthcoming papers, we will demonstrate the numerical simulations with *three-phase* composites containing randomly located and interacting aligned circular fibers with *distinct* elastic properties and sizes.

Acknowledgments This work was in part sponsored by the Faculty Research Grant of the Academic Senate of UCLA under fund number 4-592565-19914 and in part by Bellagio Engineering.

References

1. Hashin, Z., Shtrikman, S.: On some variational principles in anisotropic and nonhomogeneous elasticity. J. Mech. Phys. Solids **10**, 335–342 (1962)
2. Hashin, Z., Shtrikman, S.: A variational approach to the theory of the elastic behavior of multiphase materials. J. Mech. Phys. Solids **11**, 127–140 (1962)
3. Hill, R.: Theory of mechanical properties of fiber-strengthened materials: I. Elastic behavior. J. Mech. Phys. Solids **12**, 199–212 (1964)
4. Hill, R.: Theory of mechanical properties of fiber-strengthened materials: II. Inelastic behavior. J. Mech. Phys. Solids **12**, 213–218 (1964)
5. Hashin, Z., Rosen, B.W.: The elastic moduli of fiber-reinforced materials. J. Appl. Mech. **31**, 223–232 (1964)
6. Hashin, Z.: On elastic behavior of fiber reinforced materials of arbitrary transverse phase geometry. J. Mech. Phys. Solids **13**, 119–134 (1965)
7. Walpole, L.J.: On bounds for overall elastic moduli of inhomogeneous systems: I. J. Mech. Phys. Solids **14**, 151–162 (1966)
8. Walpole, L.J.: On bounds for overall elastic moduli of inhomogeneous Systems: II. J. Mech. Phys. Solids **14**, 289–301 (1966)
9. Walpole, L.J.: On the overall elastic moduli of composite materials. J. Mech. Phys. Solids **17**, 235–251 (1969)
10. Hashin, Z.: Theory of fiber reinforced materials. NASA CR-1974 (1972)
11. Silnutzer, N.: Effective Constants of Statistically Homogeneous Materials. Ph.D. thesis, University of Pennsylvania (1972)
12. Milton, G.W.: Bounds on the elastic and transport properties of two-component composites. J. Mech. Phys. Solids **30**, 177–191 (1982)
13. Milton, G.W., Phan-Thien, N.: New bounds on effective elastic moduli of two-component materials. Proc. R. Soc. A **380**, 305–331 (1982)
14. Torquato, S., Lado, F.: Improved bounds of the effective elastic moduli of random arrays of cylinders. J. Appl. Mech. **59**, 1–6 (1992)
15. Hill, R.: Theory of mechanical properties of fiber-strengthened materials: III. Self-consistent model. J. Mech. Phys. Solids **13**, 189–198 (1965)
16. Hill, R.: A self-consistent mechanics of composite materials. J. Mech. Phys. Solids **13**, 213–222 (1965)
17. Christensen, R.M., Lo, K.H.: Solutions for effective shear properties in three phase sphere and cylinder models. J. Mech. Phys. Solids **27**, 315–330 (1979)
18. Mori, T., Tanaka, K.: Average stress in matrix and average elastic energy of materials with misfitting inclusions. Acta Metall. **21**, 571–574 (1973)

19. Benveniste, Y.: A new approach to the application of Mori–Tanaka's theory in composite materials. Mech. Mater. **6**, 147–157 (1987)
20. Weng, G.J.: The theoretical connection between Mori–Tanaka's theory and the Hashin–Shtrikman–Walpole bounds. Inter. J. Eng. Sci. **28**, 1111–1120 (1990)
21. Eshelby, J.D.: The determination of the elastic field of an ellipsoidal inclusion, and related problems. Proc. R. Soc. Lond. A **241**, 376–396 (1957)
22. Mura, T.: Micromechanics of Defects in Solids. 2nd edn. Kluwer, The Netherlands (1987)
23. Honein, E.: Multiple Inclusions in Elastostatics. Ph.D. dissertation at Stanford University (1991)
24. Nemat-Nasser, S., Hori, M.: Micromechanics: Overall Properties of Heterogeneous Materials. Elsevier, The Netherlands (1993)
25. Ju, J.W., Chen, T.M.: Micromechanics and effective moduli of elastic composites containing randomly dispersed ellipsoidal inhomogeneities. Acta Mech. **103**, 103–121 (1994)
26. Ju, J.W., Chen, T.M.: Effective elastic moduli of two-phase composites containing randomly dispersed spherical inhomogeneities. Acta Mech. **103**, 123–144 (1994)
27. Ju, J.W., Zhang, X.D.: Micromechanics and effective transverse elastic moduli of composites with randomly located aligned circular fibers. Int. J. Solids Struct. **35**(9–10), 941–960 (1998)
28. Ju, J.W., Yanase, K.: Micromechanics and effective elastic moduli of particle-reinforced composites with near-field particle interactions. Acta Mech. **215**(1), 135–153 (2010)
29. Ju, J.W., Yanase, K.: Micromechanical effective elastic moduli of continuous fiber-reinforced composites with near-field fiber interactions. Acta Mech. **216**(1–4), 87–103 (2011)
30. Lin, P.J., Ju, J.W.: Effective elastic moduli of three-phase composites with randomly located and interacting spherical particles of distinct properties. Acta Mech. **208**, 11–26 (2009)
31. Adams, D.F., Crane, D.A.: Finite element micromechanical analysis of a unidirectional composite including longitudinal shear loading. Comput. Struct. **18**(6), 1153–1165 (1984)
32. Nimmer, R.P., Bankert, R.J., Russell, E.S., Smith, G.A., Wright, P.K.: Micromechanical modeling of fiber/matrix interface effects in transversely loaded SiC/Ti-6-4 metal matrix composites. J. Comp. Tech. Res. JCTRER **13**, 3–13 (1991)
33. Doghri, I., Friebel, C.: Effective elasto-plastic properties of inclusion-reinforced composites. Study of shape, orientation and cyclic response. Mech. Mater. **37**, 45–68 (2005)
34. Ju, J.W., Chen, T.M.: Micromechanics and effective elastoplastic behavior of two-phase metal matrix composites. Trans ASME, J. Eng. Mater. Tech. **116**, 310–318 (1994)
35. Ju, J.W., Tseng, K.H.: Effective elastoplastic behavior of two-phase ductile matrix composites: a micromechanical framework. Int. J. Solids Struct. **33**, 4267–4291 (1996)
36. Ju, J.W., Tseng, K.H.: Effective elastoplastic algorithms for ductile matrix composites. J. Eng. Mech. ASCE **123**, 260–266 (1997)
37. Ju, J.W., Zhang, X.D.: Effective elastoplastic behavior of ductile matrix composites containing randomly located aligned circular fibers. Int. J. Solids Struct. **38**, 4045–4069 (2001)
38. Ju, J.W., Sun, L.Z.: Effective elastoplastic behavior of metal matrix composites containing randomly located aligned spheroidal inhomogeneities. Part I: micromechanics-based formulation. Int. J. Solids Struct. **38**(2), 183–201 (2001)
39. Sun, L.Z., Ju, J.W.: Effective elastoplastic behavior of metal matrix composites containing randomly located aligned spheroidal inhomogeneities. Part II: applications. Int. J. Solids Struct. **38**(2), 203–225 (2001)
40. Ju, J.W., Sun, L.Z.: A novel formulation for the exterior-point Eshelby's tensor of an ellipsoidal inclusion. J. Appl. Mech. ASME **66**, 570–574 (1999)
41. Ju, J.W., Lee, H.K.: A micromechanical damage model for effective elastoplastic behavior of ductile matrix composites considering evolutionary complete particle debonding. Comput. Methods Appl. Mech. Eng. **183**, 201–222 (2000)
42. Ju, J.W., Lee, H.K.: A micromechanical damage model for effective elastoplastic behavior of partially debonded ductile matrix composites. Int. J. Solids Struct. **38**, 6307–6332 (2001)
43. Sun, L.Z., Ju, J.W., Liu, H.T.: Elastoplastic modeling of metal matrix composites with evolutionary particle debonding. Mech. Mater. **35**, 559–569 (2003)
44. Sun, L.Z., Liu, H.T., Ju, J.W.: Effect of particle cracking on elastoplastic behaviour of metal matrix composites. Int. J. Numer. Meth. Eng. **56**, 2183–2198 (2003)
45. Liu, H.T., Sun, L.Z., Ju, J.W.: An interfacial debonding model for particle-reinforced composites. Int. J. Damage Mech. **13**, 163–185 (2004)
46. Liu, H.T., Sun, L.Z.: Effects of thermal residual stresses on effective elastoplastic behavior of metal matrix composites. Int. J. Solids Struct. **41**, 2189–2203 (2004)
47. Ko, Y.F.: Effective Elastoplastic-Damage Model for Fiber-Reinforced Metal Matrix Composites with Evolutionary Fibers Debonding. Ph.D. Dissertation, University of California, Los Angeles (2005)
48. Ju, J.W., Ko, Y.F., Ruan, H.N.: Effective elastoplastic damage mechanics for fiber reinforced composites with evolutionary complete fiber debonding. Int. J. Damage Mech. **15**(3), 237–265 (2006)
49. Liu, H.T., Sun, L.Z., Ju, J.W.: Elastoplastic modeling of progressive interfacial debonding for particle-reinforced metal matrix composites. Acta Mech. **181**(1–2), 1–17 (2006)
50. Ju, J.W., Ko, Y.F., Ruan, H.N.: Effective elastoplastic damage mechanics for fiber reinforced composites with evolutionary partial fiber debonding. Int. J. Damage Mech. **17**(6), 493–537 (2008)
51. Ju, J.W., Ko, Y.F.: Micromechanical elastoplastic damage modeling of progressive interfacial arc debonding for fiber reinforced composites. Int. J. Damage Mech. **17**, 307–356 (2008)
52. Ju, J.W., Yanase, K.: Elastoplastic damage micromechanics for elliptical fiber composites with progressive partial fiber debonding and thermal residual stresses. Theor. Appl. Mech. **35**(1–3), 137–170 (2008)
53. Lee, H.K., Ju, J.W.: 3-D micromechanics and effective moduli for brittle composites with randomly located interacting microcracks and inclusions. Int. J. Damage Mech. **17**(5), 377–417 (2008)

54. Ju, J.W., Ko, Y.F., Zhang, X.D.: Multi-level elastoplastic damage mechanics for elliptical fiber reinforced composites with evolutionary complete fiber debonding. Int. J. Damage Mech. **18**(5), 419–460 (2009)
55. Ju, J.W., Yanase, K.: Micromechanical elastoplastic damage mechanics for elliptical fiber-reinforced composites with progressive partial fiber debonding. Int. J. Damage Mech. **18**(7), 639–668 (2009)
56. Ju, J.W., Yanase, K.: Size-dependent probabilistic micromechanical damage mechanics for particle reinforced metal matrix composites. Int. J. Damage Mech. **20**(7), 1021–1048 (2011)
57. Hansen, J.P., McDonald, I.R.: Theory of Simple Liquids. Academic Press, New York (1986)
58. Zhao, Y.H., Tandon, G.P., Weng, G.J.: Elastic moduli for a class of porous materials. Acta Mech. **76**, 105–131 (1989)
59. Kondo, K., Saito, N.: The influence of random fiber packing on the elastic properties of unidirectional composites. In: Composites '86: Recent Advances in Japan and the United States, Proceeding of Japan-U.S. CCM-III (1986)
60. Uemura, M., Yamawaki, K., Abe, S., Iyama, H.: On the stiffness of filament wound materials (in Japanese). Bull. Inst. Space Aeronaut. Sci. Univ. Tokyo **4**(3B), 448–463 (1968)
61. Christensen, R.M.: Effective viscous flow properties for fiber suspensions under concentrated conditions. J. Rheol. **37**, 103–121 (1993)